Dissolution Behavior of Ureolytic Biocementation: Physical Experiments and Reactive Transport Modeling

Bruna G. O. Ribeiro, S.M.ASCE[1]; and Michael G. Gomez, M.ASCE[2]

Abstract: Microbially induced calcite precipitation (MICP) is a promising bio-mediated cementation process that can improve the engineering properties of granular soils through the precipitation of calcium carbonate on soil particle surfaces and contacts. The process offers an environmentally conscious alternative to conventional soil improvement technologies which primarily rely on the use of portland cement and high mechanical energy. As the technology transitions towards field-scale application, an improved understanding of the chemical permanence of MICP will be critical towards identifying favorable applications, predicting long-term engineering behaviors, and evaluating life-cycle environmental impacts. In this study, a series of soil column and batch reaction experiments were performed in tandem with reactive transport numerical modeling to investigate the dissolution behavior of biocementation generated via microbial ureolysis. Five soil column experiments containing a poorly graded sand were treated identically to achieve average $CaCO_3$ contents near 5% by mass and were then subjected to either 0, 5, 10, 20, or 50 identical acidic dissolution injections. A dissolution kinetic model was calibrated independently to batch experiments involving similar solutions and was incorporated into a reactive transport model to forward predict degradation expected during soil column experiments. Spatial and temporal changes in biocementation dissolution were assessed using geophysical and geochemical measurements and observations were compared to those obtained from reactive transport simulations. Results indicate that existing kinetic models can successfully capture the dissolution behavior of ureolytic biocementation; however, model parameters may require site-specific calibration using soil column experiments. Outcomes are expected to significantly improve our understanding of the dissolution kinetics of biocementation, its effects on soil mechanical properties, and provide approaches through which the chemical resilience of MICP soil improvement can be evaluated. **DOI: 10.1061/JGGEFK.GTENG-11275.**

Introduction

Traditional geotechnical ground improvement methods oftentimes rely on the use of high mechanical energy and/or energy intensive materials, such as portland cement, to improve soil engineering properties (DeJong et al. 2010; Pinske 2011; Mitchell and Kelly 2013; Raymond et al. 2017). Recognizing the environmental impacts of conventional technologies, societal interest and demand for sustainable ground improvement methods has increased significantly in recent years (Karol 2003; DeJong et al. 2013, 2022). Bio-mediated soil improvement technologies offer novel approaches to improve soil engineering characteristics while simultaneously affording the potential to achieve significant environmental benefits when compared to other business-as-usual ground improvement techniques (Seagren and Aydilek 2010; DeJong et al. 2013, 2022). Microbially induced calcite precipitation (MICP) is one such technology, that can improve the engineering properties of soils through the precipitation of calcium carbonate ($CaCO_3$) minerals on soil particle surfaces and contacts (Ferris et al. 1997; Stocks-Fischer et al. 1999; DeJong et al. 2006; Martinez and DeJong 2009; and others).

The MICP process is made possible by ureolytic bacteria, which hydrolyze urea in the presence of calcium (Ca^{2+}), thereby generating aqueous carbonate species and initiating $CaCO_3$ precipitation. Among other mechanical enhancements, MICP can increase the initial shear stiffness, peak shear strength, and liquefaction resistance of soils, while reducing soil porosity and hydraulic conductivity (DeJong et al. 2006; Tobler et al. 2012; Al Qabany and Soga 2014; Martinez et al. 2013; Montoya and DeJong 2015; Gomez and DeJong 2017; Lee et al. 2022). Potential engineering applications include liquefaction mitigation, slope stability improvement, subsurface flow manipulation, and contaminant immobilization, among other uses (Fujita et al. 2004; DeJong et al. 2006; Montoya et al. 2013; Phillips et al. 2016; Gomez and DeJong 2017). While significant advances in the technology have been made with respect to application techniques (O'Donnell et al. 2017; Gomez et al. 2018), up-scaling of the process towards practical applications (van Paassen 2011; Smith et al. 2012; Gomez et al. 2015, 2017; San Pablo et al. 2020), reactive transport modeling of MICP treatment processes (Ebigbo et al. 2012; Martinez et al. 2014; Nassar et al. 2018, Minto et al. 2019), the characterization of post-treatment engineering behaviors (Montoya and DeJong 2015; Zamani and Montoya 2018; Lee et al. 2022), and the susceptibility of biocementation to select extreme conditions including freeze-thaw cycles and acid rain (Cheng et al. 2013; Gowthaman et al. 2020a, b; Sun et al. 2021), there remains limited understanding of the factors that control biocementation material properties and the processes by which biocemented soils can chemically degrade over time in the subsurface following treatment application. Although almost no research until now has investigated the chemical permanence of biocementation, it is anticipated that the mineralogy, morphology, and dissolution kinetics of generated $CaCO_3$

[1]Ph.D. Student, Dept. of Civil and Environmental Engineering, Univ. of Washington, Seattle, WA 98195. ORCID: https://orcid.org/0000-0003-3501-9089. Email: brunagr@uw.edu

[2]Assistant Professor, Dept. of Civil and Environmental Engineering, Univ. of Washington, Seattle, WA 98195 (corresponding author). ORCID: https://orcid.org/0000-0002-4464-5447. Email: mggomez@uw.edu

Note. This manuscript was submitted on August 24, 2022; approved on April 19, 2023; published online on June 24, 2023. Discussion period open until November 24, 2023; separate discussions must be submitted for individual papers. This paper is part of the ***Journal of Geotechnical and Geoenvironmental Engineering***, © ASCE, ISSN 1090-0241.

precipitation will all influence the long-term geochemical resilience of biocemented soils.

MICP is commonly referred to as generating calcite minerals; however, produced calcium carbonate can exist as a variety of different crystalline polymorphs including aragonite, vaterite, ikaite, and calcite as well as poorly structured amorphous $CaCO_3$ (Plummer and Busenberg 1982; Sposito 2008). Each of these polymorphs have differing morphologies and physicochemical properties and thus the specific minerals generated during MICP may significantly alter the long-term chemical and mechanical stabilities of the material. For example, the solubility product (K_{sp}) of $CaCO_3$ polymorphs can vary widely with ikaite, vaterite, aragonite, and calcite having K_{sp} values of $10^{-6.62}$, $10^{-7.91}$, $10^{-8.34}$, and $10^{-8.48}$, respectively (Plummer and Busenberg 1982; Gal et al. 2002; APHA 2005). Recent studies have investigated how environmental conditions and treatment techniques can impact the mineralogy and morphology of ureolytic biocementation, in an effort to better understand material permanence. Burdalski and Gomez (2020) examined the impact of variations in bulk ureolytic activity, ureolytic cell densities, and applied urea-to-calcium concentration ratios on the mineralogy of resulting biocementation. Burdalski et al. (2022) further examined the effect of variations in groundwater and seawater ions (Mg^{2+}, Sr^{2+}, SO_4^{2-}, and Na^+) and parent soil minerals on generated precipitate composition as well as reaction kinetics. In 78 additional experiments involving changes in surrounding geochemical conditions, calcite was found to be the predominant mineral polymorph with relative percentages of calcite exceeding 80% by mass in all precipitates (Burdalski 2020). Although the mineralogy and morphology of biocementation will likely be governed by both the employed treatment techniques and site-specific conditions, other past investigations (Burbank et al. 2011; Almajed 2017; Khodadadi et al. 2017; Mu et al. 2021) have also qualitatively observed the predominance of calcite minerals in ureolytic biocementation. Collectively, these insights suggest that the long-term chemical permanence of biocementation may be largely governed by the dissolution kinetics of calcite with other polymorphs having a more minor role.

Numerous past studies have examined the dissolution behavior of both naturally occurring and abiotically generated $CaCO_3$ minerals (Sjöberg and Rickard 1984; Morse and Arvidson 2002; Cubillas et al. 2005; Gehlen et al. 2005; Colombani 2016; and others) and have yielded important insights regarding the expected dissolution kinetics and geochemical behaviors of these minerals. Significant changes in the dissolution behavior of $CaCO_3$ minerals have been observed as a function of the pH and temperature of surrounding solutions (Sjöberg and Rickard 1984). Accordingly, two different dissolution kinetic models have been proposed to describe the dissolution behavior of $CaCO_3$ as a function of the pH of surrounding solutions with behaviors being described as either "chemically controlled" or "diffusion-controlled." When the pH of the surrounding solutions exceeds 5.5, the rate of $CaCO_3$ dissolution is largely chemically controlled with dissolution rates proportional to the surrounding solution's saturation index, which can be described as the ratio of the product of the activities of calcium and carbonate to the $CaCO_3$ mineral solubility product. Eq. (1) presents the chemically controlled dissolution kinetic expression wherein r_c is the dissolution rate, k_c is a dissolution rate constant, A_c is the mineral specific surface area, n is the reaction order, K_{sp} is the solubility product of the mineral, and (Ca^{2+}) and (CO_3^{2-}) are the activities of calcium and carbonate ions, respectively (Morse and Berner 1972). Conversely, under more acidic conditions (pH < ≈4), $CaCO_3$ dissolution rates are largely diffusion-controlled with dissolution rates instead dependent on the pH of surrounding solutions. Eq. (2) presents the diffusion-controlled dissolution kinetic expression, wherein r_c is the dissolution rate, k_c is a dissolution rate constant, A_c is the mineral specific surface area, (H^+) is the activity of hydrogen ions obtained from the solution pH, and n is the reaction order (Sjöberg and Rickard 1984)

$$r_c = k_c A_c \left(1 - \frac{(Ca^{2+})(CO_3^{2-})}{K_{sp}}\right)^n \tag{1}$$

$$r_c = k_c A_c (H^+)^n \tag{2}$$

While these studies have improved our fundamental understanding of the dissolution behavior of $CaCO_3$ minerals synthesized in the laboratory and present within geological samples, the applicability of these frameworks towards capturing the chemical degradation behavior of biocementation has remained relatively unexplored. Ribeiro and Gomez (2022) recently performed a series of batch experiments to investigate the ability of the existing chemically controlled and diffusion-controlled dissolution kinetic models to approximate the dissolution behavior of biocemented sands when exposed to various acidic solutions. These experiments suggested that existing kinetic models can be used to reasonably approximate the dissolution behavior of biocementation under a range of different conditions, including initial solution pH values between 2.2 and 5.6 and acid normality values between 10 and 50 mM, with the consistency between modeled and experimental trends dependent on initial solution pH and solution buffering capacity. Despite these recent advances in our understanding of biocementation mineralogy and dissolution kinetics, knowledge gaps have persisted regarding whether or not these modeling approaches can capture the dissolution behavior of biocementation under conditions more representative of in situ soils and if dissolution kinetic parameters can be successfully determined from independent batch experiments.

In this study, a series of soil column and batch experiments were performed in combination with reactive transport numerical modeling to investigate the dissolution behavior of $CaCO_3$ biocemented soils. Five soil columns containing poorly graded sand received identical MICP treatment injections intended to augment columns with ureolytic *Sporosarcina pasteurii* (*S. pasteurii*) cells and achieve relatively uniform soil $CaCO_3$ contents near 5% by mass. Following cementation, columns received daily acidic dissolution solution injections intended to characterize the spatial and temporal progression of $CaCO_3$ dissolution at various points in time. During all treatments, nondestructive shear wave velocity (V_s) measurements were obtained at three locations within each column and aqueous chemical measurements were performed to track changes in ureolytic activity, cementation progression, and subsequent dissolution-induced mechanical and geochemical changes. Following all dissolution injections, columns were destructively sampled to determine soil $CaCO_3$ content distributions and scanning electron microscope (SEM) imaging and x-ray diffraction (XRD) analyses were conducted to examine potential changes in precipitate mineralogy and morphology during the dissolution process. In parallel with soil column experiments, a one-dimensional advective-dispersive reactive transport model was implemented using the geochemical code PHREEQC (Parkhurst and Appelo 2013) to forward predict dissolution behaviors expected during column experiments using kinetic parameters determined from independent dissolution batch experiments. Following all soil column experiments, model predictions and experimental results were compared, and model parameters were further modified to better approximate experimental observations. Finally, recommendations for future experimentation and model calibration are provided with the ultimate goal of providing rational and practical numerical approaches for predicting biocementation permanence under varying site-specific geochemical conditions.

Materials and Methods

Dissolution Batch Experiments

Batch experiments were performed to examine the dissolution behavior of biocemented soils with the specific aim of calibrating existing dissolution kinetic models to capture changes in aqueous chemistry during the dissolution process. All batch experiments were completed following procedures similar to Ribeiro and Gomez (2022) and involved mixing 20 grams of dry biocemented sand samples ($CaCO_3$ content of 5.0% by mass) with 100 mL of dissolution solutions containing 50 mM acetic acid (pKa = 4.75) and 100 mM sodium acetate ($pH_{initial} = 4.95$). All biocemented sand samples were obtained from previous soil column experiments (Lee et al. 2019) involving a poorly graded concrete sand material ($D_{50} \approx 1.07$ mm, fines content $\approx 1.1\%$). During batch experiments, dry sand samples were placed in glass bottles, dissolution solutions were added, and bottles were sealed and continuously agitated for 48 h using a double-orbital shaker (shaking speed of 150 rpm). During the dissolution process, pH measurements were performed, and aqueous samples were obtained 30, 60, 120, 240, 360, 480, 600, 1,200, 1,800, 5,400, and 172,800 s after initial mixing. Aqueous samples were 500 μL in volume and were filtered immediately after collection using 0.22-μm cellulose acetate centrifuge filters to remove solids (Corning Inc., Corning, New York). Samples were immediately frozen after filtering until thawing for aqueous calcium measurements. Two replicate batch experiments were performed to assess repeatability. Although other dissolution solutions could have been considered, this particular solution was selected for several reasons including: (1) the solution consisted of a weak organic acid, which was anticipated to be more representative of acidic conditions expected for in situ soils wherein biological activity and degradation of organic carbon may generate low concentrations of organic acids and solutions that are only slightly undersaturated with respect to $CaCO_3$; (2) the higher buffering capacity of this solution allowed for significant dissolution to proceed over experimentally practical timeframes (e.g., 50 days) in contrast to much longer geological timeframes (e.g., years) which would be needed to observe dissolution for solutions that were prepared closer to equilibrium with $CaCO_3$; (3) an existing kinetic model was shown to well approximate the dissolution behavior of biocemented sands subjected to this solution in previous batch experiments (Ribeiro and Gomez 2022); and (4) the use of this solution allowed for sufficient dissolution of $CaCO_3$ during batch experiments such that dissolution behaviors could be characterized using Ca^{2+} measurements. Although it is acknowledged that this solution may not be representative of all site-specific geochemical conditions, the use of this solution provided the opportunity to better understand biocementation dissolution progression, the metrics by which biocementation degradation can be monitored, and allowed for the development of numerical modeling approaches which may afford the ability to predict how biocemented materials may degrade under site-specific conditions (i.e., groundwater compositions, flow regimes).

Soil Column Experiments

Five soil columns (14.94 cm length, 7.62 cm inner diameter) were prepared using Ottawa F-65 sand placed at a relative density (D_r) of $\approx$40%. Ottawa F-65 sand (US Silica, Ottawa, Illinois) is a poorly graded sand (SP) [ASTM D2487 (ASTM 2017)] that has a D_{50} of $\approx$0.21 mm, coefficient of uniformity of 1.77, coefficient of curvature of 1.08, and no fines. Minimum and maximum void ratios for this material were determined to be 0.51 and 0.78 (Carey et al. 2020), respectively, following procedures outlined in ASTM D4253 and D4254 (ASTM 2016a, b). Sand materials were prepared using six equal lifts that were dry-tamped following placement and scarified between lifts to limit potential density differences between lifts. Polyethylene plastic discs with pore sizes between 125 and 195 μm (Porex Corp., Fairburn, Georgia) were placed at the top and bottom of the columns as filters. Columns had an average porosity of 0.36 and pore volumes (PVs) near 250 mL. All columns received treatments from the bottom upwards in order to maintain saturation during treatments. Treatments were applied through PFTE column end caps that included nylon barbed fittings which were connected to PVC tubing used to inject solutions and allow for drainage of produced effluent. A total stress of 100 kPa was applied to all columns from top caps using spring-loaded loading reaction frames. Columns had three bender elements sensor pairs and three aqueous sampling ports located at distances of 3.5, 8.6, and 13.7 cm from the injection location at the base of columns in order to monitor changes in soil shear stiffnesses and aqueous reaction chemistry spatially and temporally. All columns were saturated with deionized water for at least 2 h prior to the passive tracer test injections. Fig. 1 provides an overview of column set-ups including the locations of bender element sensors, sampling ports, and the treatment application system.

Fig. 1. (a) Overview of soil column experiments including bender element sensors, sampling ports, and the treatment application system; and (b) close-up view of a single soil column with top, middle, and bottom measurement locations, the injection location, and loading frame noted.

Saturation and Bromide Passive Tracer Testing

Passive tracer testing was performed to characterize the advective-dispersive transport properties of soil columns both (1) prior to all MICP treatments; and (2) immediately prior to all dissolution injections and following cementation treatments and post-cementation rinse injections. During passive tracer testing, 750 mL [≈3 pore volume (PV)] of NaBr solutions were injected followed by a 750 mL injection of deionized water at a constant flow rate of 20 mL/min to examine how a conservative tracer was transported through columns. Initial passive tracer tests were performed using 15 mM NaBr prepared in deionized water. However, post-cementation passive tracer tests were completed using 200 mM NaBr solutions prepared in deionized water that was previously equilibrated with $CaCO_3$ solids for at least 2 h and passed through a 0.22-μm vacuum filter in order to provide greater contrast with background solution conductivities and mitigate potential dissolution. During injections, soil column effluent solutions were sampled once every 50 mL (≈ 0.33 PV) and solution conductivities were measured, indicative of passive ion concentrations. All measurements were normalized by the initial conductivity (C_0) of injected NaBr solutions ($C_0 = 1{,}682$ μS/cm for 15 mM NaBr; $C_0 = 19.9$ mS/cm for 200 mM NaBr), in order to determine normalized Br^- concentrations (C/C_0) as a function of injected volume.

Cell Preparation

Sporosarcina pasteurii (*S. pasteurii*, ATCC 11859) cells were cultured in sterile ATCC 11859 growth media [0.13 M tris base, 20 g/L yeast extract, 10 g/L $(NH_4)_2SO_4$, pH-adjusted to 9.0, autoclaved at 121°C] which was inoculated with a frozen stock culture that had been stored at −80°C. Inoculated growth media was incubated at 30°C using a double-orbital shaker at a shaking speed of 150 rpm for 48 h. After incubation, the growth medium was centrifuged (1,972 g, 10 min) and cells were rinsed twice with sterile isotonic saline (9 g/L NaCl). Concentrated *S. pasteurii* cell pellets were then obtained by adding 10 mL of sterile isotonic saline to rinsed cells and mixing thoroughly. The optical density at a wavelength of 600 nm (OD_{600}) of the concentrated *S. pasteurii* cell pellets was measured with a microplate spectrophotometer and determined that pellets had a cell density of 1.77×10^9 cell/mL following a total direct cell count to OD_{600} correlation (Burdalski et al. 2022). Cell pellets were then diluted in an augmentation solution (100 mM ammonium chloride, 10 mM urea, 0.2 g/L yeast extract) to achieve a total cell density of 4.37×10^7 cell/mL.

Treatment Solution Injections

All columns received daily treatments in a series of five different phases: (1) augmentation; (2) cementation; (3) post-cementation rinsing; (4) post-cementation passive tracer testing; and (5) dissolution injections. All treatments were identical between columns with the exception of dissolution injections, during which varying numbers of identical dissolution injections were applied between columns. Columns CD0, CD5, CD10, CD20, and CD50 received 0, 5, 10, 20, and 50 dissolution injections, respectively, to examine dissolution progression with respect to time. Table 1 summarizes all treatment solutions and injections including applied injection volumes and frequencies and solution chemical compositions. All injections were completed at a flow rate of 20 mL/min (0.08 PV/min).

Immediately following initial passive tracer testing, all columns received identical augmentation injections intended to augment soil columns with *S. pasteurii* cells and achieve sufficient ureolytic activity to enable biocementation. One liter augmentation solution volumes (≈4PV), which included 4.36×10^7 cells/mL of

Table 1. Summary of applied treatment solution injections and chemical compositions

	Applied injections		Chemical composition									
Solution type	Injection volume per column	Injection frequency	*S. pasteurii* cell density (cells/mL)	Ammonium chloride (mM)	Urea (mM)	Yeast extract (g/L)	Calcium chloride (mM)	Acetic acid (mM)	Sodium acetate (mM)	Sodium bromide (mM)	Other	Initial pH
Pre-treatment passive tracer	3 PV	Once	—	—	—	—	—	—	—	15	—	7.95
Augmentation	4 PV	Once	4.37×10^7	100	10	0.2	—	—	—	—	—	6.4
Cementation	1.5 PV	Once daily for 10 days	—	100	250	0.2	250	—	—	—	—	7.5
Post-cementation rinse	6 PV	Once	—	—	—	—	—	—	—	—	Equilibrated with 0.2 g/L $CaCO_3$ and 0.2 μm-filtered	8.74
Post-cementation passive tracer	3 PV	Once	—	—	—	—	—	—	—	200	Equilibrated with 0.2 g/L $CaCO_3$ and 0.2 μm-filtered	8.69
Dissolution	1 PV	Once daily for 0, 5, 10, 20, or 50 days	—	—	—	—	—	50	100	—	—	4.97

S. pasteurii cells, were applied to each column and were injected in five different phases intended to achieve spatially uniform cell distributions in all columns. Injection procedures were similar to Lee et al. (2022) and proceeded as follows: (1) 250 mL (≈1PV) were injected from bottom to top with the resulting effluent discarded; (2) 250 mL (≈1PV) were injected from bottom to top with the resulting effluent retained; (3) 500 mL (≈2PV) were injected from top to bottom with the resulting effluent retained; (4) retained solutions were homogenized and 250 mL (≈1PV) of this solution was injected from bottom to top with the resulting effluent retained; and (5) solutions were homogenized again and 500 mL (≈2PV) was injected from top to bottom with the resulting effluent retained. Solution OD_{600} measurements were performed to determine the total cell densities present in augmentation solutions and the quantity of cells retained in column pore fluids and attached to soil particles as follows: (1) the total cells introduced to each column from augmentation solutions were determined from OD_{600} measurements and known injection volumes; (2) the cells retained within each column were determined by measuring the OD_{600} of the remaining augmentation solutions after all injections; and (3) column pore fluids were sampled from the center of each column to determine the number of cells present in the aqueous phase, with the cells attached to soil particle surfaces estimated from the difference between the total cells retained within columns and those quantified in the aqueous phase.

Following augmentation, all columns received ten 375 mL (≈1.5PV) daily cementation injections intended to achieve $CaCO_3$ contents near 5% by mass in all columns. Cementation solutions contained 250 mM urea, 250 mM calcium chloride, 100 mM ammonium chloride, and 0.2 g/L yeast extract following similar solutions from previous studies (Gomez et al. 2018; Lee et al. 2019; San Pablo et al. 2020; and others) and were applied from the bottom of columns upwards. Twenty-four hours after the last cementation injection, all columns received post-cementation rinse injections to remove generated aqueous by-products (e.g., total carbonate species, total NH_4^+) and prepare columns for post-cementation passive tracer testing. During rinsing, 1.5 L (≈6PV) of a solution previously equilibrated with $CaCO_3$ was applied to avoid potential dissolution of biocementation. The $CaCO_3$-equilibrated solution was prepared by allowing 0.2 g/L of solid reagent-grade $CaCO_3$ (≥99.0%, Thermo Fisher Scientific, Waltham, MA) to equilibrate with deionized water over 2 h and removing all mineral solids using a 0.22-μm filter. After rinsing, post-cementation passive tracer testing was performed to examine potential changes in column advective-dispersive transport following biocementation. Following passive tracer testing, column CD0, which received no dissolution injections, was destructively sampled. Columns CD5 through CD50, however, received daily 1 PV dissolution solution injections that proceeded for various durations between 5 and 50 days. Dissolution solutions were identical to batch experiments (50 mM acetic acid, 100 mM sodium acetate, $pH_{initial} \approx 4.97$). All dissolution injections were applied to columns from the bottom upwards. Twenty-four hours after the last dissolution injection, the columns were destructively sampled.

Aqueous Sampling

Aqueous samples (≈2 mL) were obtained from all columns at various times during treatments to monitor changes in ureolytic activity as well as cementation and dissolution progression spatially and temporally. Samples were collected from all sampling ports before and 24 h after all cementation injections. For cementation injections 1, 5, and 10, additional samples were also collected from all sampling ports 2, 4, and 8 h after injection to monitor changes in ureolysis and precipitation kinetics. During dissolution, samples were obtained before and 24 h after injection for dissolution injections 1, 5, 10, 15, 20, 25, 30, 45, and 50. During these same dissolution injections, effluent solutions exiting columns were collected and homogenized, pH measurements were completed, and bulk samples of column effluent solutions were analyzed to track cumulative masses of Ca^{2+} removed from columns during the dissolution process. After collection, all samples were frozen until thawing for subsequent chemical measurements.

Aqueous Chemical Measurements

Solution pH measurements were performed using a semi-micro pH electrode and meter system (Thermo Fisher Scientific, Waltham, Massachusetts) that had ±0.01 pH unit accuracy. Aqueous Ca^{2+} measurements were completed using a QuantiChrom calcium assay kit (BioAssay Systems, Hayward, California). Ca^{2+} assay samples were diluted in water purified using a Milli-Q lab water system (MilliporeSigma, Burlington, Massachusetts) to obtain Ca^{2+} concentrations within the linear range of the assay (<5.0 mM) and a colorimetric reagent was added to samples and allowed to react for 10 min. Sample absorbances were measured using a microplate spectrophotometer at a wavelength of 612 nm and Ca^{2+} concentrations were determined from a calibration curve. Urea measurements were completed using a colorimetric urea assay modified from Knorst et al. (1997), wherein a colorimetric reagent consisting of 4% (w/v) *p*-dimethylaminobenzaldehyde and 19% (v/v) HCl in absolute ethanol was added to samples. Absorbance values were measured at 422 nm using a microplate spectrophotometer and urea concentrations were determined from a calibration curve.

Shear Wave Velocity Measurements

Shear wave velocity (V_s) measurements were completed using three bender element sensor pairs located 3.5 cm (bottom), 8.6 cm (middle), and 13.7 cm (top) from the injection location at the bases of columns (Fig. 1). Bender element transmitters were excited using a 100 Hz square wave generated using a custom data acquisition system (National Instruments Inc., Austin, Texas) and 24 V voltage supply (BK Precision Corp., Yorba Linda, California). Received signals were measured and recorded at a sampling frequency of 1 MHz using a digital oscilloscope (PicoScope Inc., Tyler, Texas). The values of V_s were determined from known sensor spacings and visual interpretations of shear wave arrival times. Measurements of V_s were completed at all column locations before and after all injections. Additional V_s measurements were also performed before and after rinse injections completed during the transition from cementation to dissolution injections.

$CaCO_3$ Content Measurements

Twenty-four hours after the last cementation (CD0) or dissolution injection (CD5, CD10, CD20, CD50), columns were sectioned along their length to obtain soil subsamples for $CaCO_3$ content measurements at varying distances from the injection location. All columns were subsampled into fifteen 1-cm length sections that were oven-dried for at least 48 h at 110°C and mixed prior to $CaCO_3$ content measurements to obtain representative subsamples. Soil $CaCO_3$ contents were determined for all samples using pressure chamber measurements following ASTM D4373 (ASTM 2014) and procedures similar to that described in Lee et al. (2022). A minimum of three $CaCO_3$ content measurements were completed for all subsamples and were then averaged. Replicate measurements differed by no more than 0.5% $CaCO_3$ by mass for the same subsample. Coefficients of variation (COV) were 5.4% on average for all measurements.

PHREEQC Geochemical Modeling

Dissolution progression during both batch and soil column experiments was modeled using the open-source geochemical code PHREEQC (Parkhurst and Appelo 2013). PHREEQC models were used to simulate changes in bulk solution chemistry including temporal changes in solution pH and aqueous Ca^{2+} concentrations, which were compared to experimental observations. For all simulations, dissolution was modeled using the chemically controlled dissolution kinetic equation [Eq. (1)], which better captured trends in time for the solution considered. In the chemically controlled dissolution kinetic, the solubility product (K_{sp}) of $CaCO_3$-based biocementation was assumed to be $10^{-8.48}$ following values measured for calcite (Stumm and Morgan 2012) and recent studies confirming the predominance of calcite minerals in biocemented sands under most reaction conditions (Gomez et al. 2019; Burdalski and Gomez 2020). Batch experiments were used to calibrate the kinetic parameters, k_cA_c and n, with expected values for these parameters informed by those from similar past studies (Cubillas et al. 2005).

Following calibration to batch experiments, the kinetic model was then used to simulate the dissolution process for the soil columns experiments. All models had an input initial soil $CaCO_3$ distribution identical to that measured in the CD0 column immediately following the cementation phase; therefore, all other prior treatment phases including augmentation and cementation treatments were not modeled. All PHREEQC soil column models consisted of 60 cells (≈0.249 cm each) and received between 0 and 50 dissolution injections that were identical to the physical experiments. Since only 15 discrete $CaCO_3$ content measurements could be obtained from each column experiment, $CaCO_3$ content measurements were representative of a 1-cm column length and were compared to the average value obtained from four cells in the numerical simulations. Prior to simulating the dissolution process, PHREEQC column models were calibrated to match one-dimensional advective-dispersive transport conditions present in column experiments by varying both the porosity (n_p) and longitudinal dispersivity (α_L) of columns to match observations from passive tracer testing. During dissolution injection simulations, soil $CaCO_3$ content spatial distributions, aqueous Ca^{2+} concentrations, pH values within columns, effluent solution aqueous Ca^{2+} concentrations, and pH values were determined for select injections. Although dissolution kinetic parameters determined from the independent batch experiments were used for initial simulations, the k_cA_c and n kinetic parameters were further modified following experiments to better match column observations and additional simulations were performed using these refined parameters.

X-Ray Diffraction Analyses

XRD analyses were performed on biocemented sand samples obtained from the bottom (3.5 cm from injection source) and top (13.7 cm from injection source) of columns in order to characterize the mineralogy of generated biocementation and examine the potential impact of dissolution injections. Prior to XRD analyses, samples were oven-dried for at least 24 h at 110°C and mixed with 5% by mass α-phase Al_2O_3 powder (Sigma Aldrich Inc., St. Louis, MO), which served as an internal standard. All materials were ground into a fine powder (particle size = 10 to 50 μm) and XRD analyses were performed using a Bruker D8 Discover X-ray powder diffractometer following procedures identical to that described in Burdalski et al. (2022). Diffraction patterns were analyzed using Diffrac.EVA XRD software (version 4.3) and the ICDD PDF2, ICDD PDF4, and COD reference diffraction databases (Bruker Corp., Billerica, MA), and semi-quantitative (SQ) analyses were performed to estimate relative abundances of $CaCO_3$ polymorphs (calcite, vaterite, aragonite).

Scanning Electron Microscope Imaging

SEM imaging was used to examine samples obtained from the bottom (3.5 cm from injection) and top (13.7 cm from injection) of columns in order to characterize potential changes in $CaCO_3$ morphology and precipitate composition resulting from the dissolution process. SEM imaging was performed using a FEI XL830 dual-beam focused ion beam scanning electron microscope (FEI Co., Hillsboro, OR) following procedures identical to that described in Burdalski et al. (2022). Energy dispersive x-ray spectroscopy (EDS) was also completed for select specimens to confirm the elemental composition of imaged precipitates.

Results and Discussion

Dissolution Batch Experiments for Kinetic Model Calibration

Fig. 2 presents aqueous Ca^{2+} concentration and solution pH measurements obtained during two dissolution batch experiments along with modeled trends obtained using the chemically controlled dissolution kinetic model [Eq. (1)] implemented in PHREEQC. Batch experiments were performed to determine unknown kinetic parameters k_cA_c and n and involved subjecting biocemented sand samples to dissolution solutions while monitoring chemical changes. At the start of the experiments, the initial pH was near 5.0 and no measurable aqueous Ca^{2+} was detected. As experiments proceeded, both Ca^{2+} concentrations and pH values increased progressively, reflective of $CaCO_3$ dissolution, with large increases in these values occurring after ≈100 s and ≈3,000 s, respectively. After 48 h, Ca^{2+} concentrations stabilized near 27 mM with final pH values slightly above 6.5. From the obtained measurements, the chemically controlled kinetic model was calibrated and k_cA_c and n values of 2×10^{-4} and 14, respectively, were selected, which minimized residual errors between modeled and observed Ca^{2+} concentrations. Such values were consistent with the k_cA_c and n values reported by Ribeiro and Gomez (2022) for similar conditions. During calibration, the approximation of Ca^{2+} concentration trends in time was prioritized over pH measurements as Ca^{2+} changes were most reflective of $CaCO_3$ mass losses during dissolution. The calibrated chemically controlled kinetic model, referred to as dissolution model 1, was able to closely approximate experimentally observed Ca^{2+} concentrations in time over the entire 48-h monitoring period. When comparing modeled pH values to experimental measurements, the model was shown to well approximate solution pH changes until ≈1,800 s, after which modeled values stabilized near 5.75 and were considerably lower than experimental values near 6.5. Collectively, these results suggested that the chemically controlled dissolution kinetic framework could be used to reasonably approximate the dissolution behavior of biocementation under batch conditions. It remained unclear, however, if the calibrated kinetic model could be used to forward predict biocementation dissolution under conditions more representative of in situ soils in soil column experiments.

Passive Tracer Testing

Following saturation of soil columns, passive tracer testing was performed to examine potential differences in advective-dispersive transport properties between columns both before and after biocementation. Fig. 3 presents normalized effluent solution conductivities (C/C_0) versus injected pore volumes (PVs) measured during

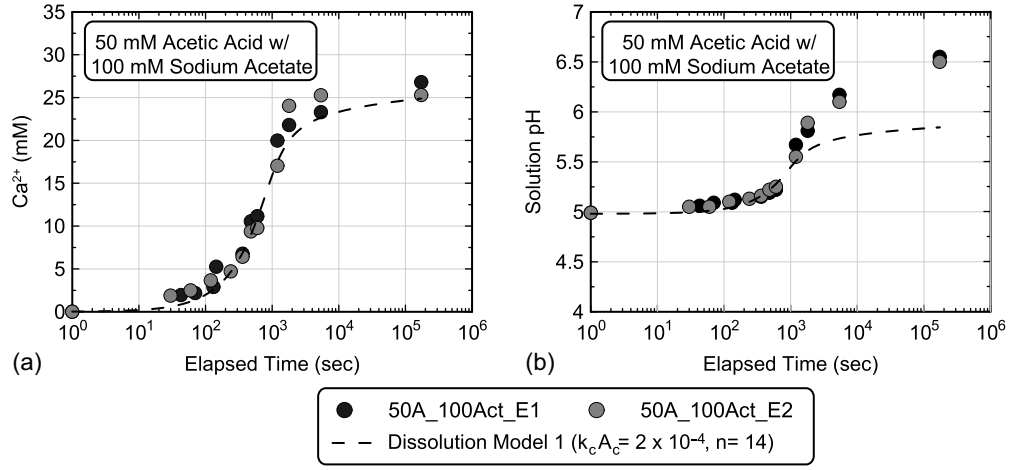

Fig. 2. Experimental measurements and modeled trends for two batch experiments involving solutions containing 50 mM acetic acid and 100 mM sodium acetate. Dissolution model 1 was calibrated to capture trends from batch experiments assuming a $k_c A_c$ value of 2×10^{-4} and n of 14. Plots present both (a) Ca^{2+} concentrations (mM); and (b) pH values versus time.

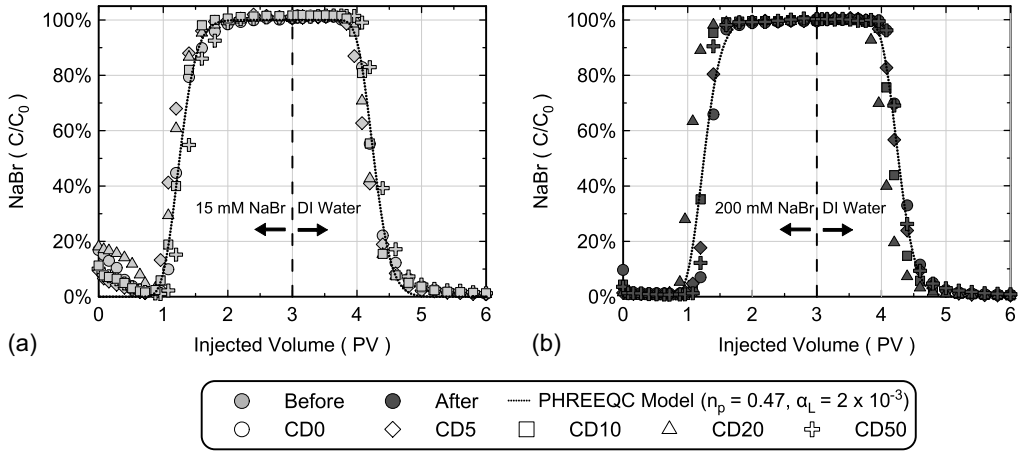

Fig. 3. Measurements of normalized solution conductivities (C/C_0) versus injected pore volumes from passive tracer tests completed for all columns (a) prior to; and (b) after biocementation treatments. Simulated trends obtained from a PHREEQC soil column model are provided which assumed a porosity (n_p) of 0.47 and a longitudinal dispersivity (α_L) of 2×10^{-3} m. C/C_0 is the measured effluent solution conductivity (C) normalized by the conductivity of the injected bromide solution (C_0).

passive tracer tests completed before [Fig. 3(a)] and after biocementation [Fig. 3(b)] along with modeled trends obtained from a calibrated soil column advective-dispersive transport model in PHREEQC. During passive tracer tests completed prior to biocementation, initial C/C_0 values were slightly elevated (<20%) due to the presence of soluble ions in column soil solutions following saturation with deionized water. C/C_0 values increased rapidly after injecting between 1 PV and 1.5 PV of the NaBr solution, however, after which C/C_0 values approached 100%. After injecting 3 PV of NaBr solutions, deionized water was then injected for an additional 3 PV and similar C/C_0 reduction behaviors were observed with values approaching <10% after injecting an additional 1.5 PV. Similar behaviors were observed for passive tracer tests completed after biocementation, although initial C/C_0 values were closer to 0%. Minimal differences in passive tracer behaviors were observed between columns before and after biocementation, suggesting that column transport properties remained comparable throughout the treatment process. In order to calibrate the advective-dispersive column transport model, the porosity (n_p) and longitudinal dispersivity (α_L) of the model were varied and determined to be 0.47 and 2×10^{-3} m, respectively, and were able to well approximate tracer behaviors both before and after biocementation. Although unexpected, the minimal effect of biocementation on column advective-dispersive transport properties was consistent with results from more recent experiments, which have shown the limited impact of MICP on soil pore structures and hydraulic conductivities when $CaCO_3$ contents are less than 10% (Baek et al. 2022; DeJong et al. 2022). Although column CD20 exhibited a slightly earlier breakthrough than other columns, indicative of a slightly smaller apparent porosity, this difference was considered in subsequent simulations and found to have no significant effects.

Ureolytic Activity and Biocementation Progression

Following passive tracer testing, all columns received augmentation injections to establish ureolytic microbial populations. Table 2

Table 2. Summary of *S. pasteurii* cells supplied and retained within columns following augmentation

	Total cells provided in augmentation solution	Cells retained in columns		Cells retained in pore fluids		Cells retained on particle surfaces	
Column	Total cells (cells)	Total cells (cells)	% of augmentation solution	Total cells (cells)	% of augmentation solution	Total cells (cells)	% of augmentation solution
CD0	4.34×10^{10}	3.52×10^{10}	81.2	9.54×10^{9}	22.0	2.57×10^{10}	59.2
CD5	4.34×10^{10}	3.49×10^{10}	80.4	9.71×10^{9}	22.4	2.52×10^{10}	58.1
CD10	4.34×10^{10}	3.52×10^{10}	81.1	9.51×10^{9}	21.9	2.57×10^{10}	59.2
CD20	4.34×10^{10}	3.46×10^{10}	79.7	1.03×10^{10}	23.7	2.43×10^{10}	56.0
CD50	4.34×10^{10}	3.49×10^{10}	80.4	1.06×10^{10}	24.4	2.43×10^{10}	56.0

summarizes the quantities of total cells that were (1) supplied in augmentation solutions; (2) retained within column pore fluids; and (3) retained on soil particle surfaces as determined by OD_{600} measurements obtained during augmentation. As shown, all columns retained approximately 80% of the total cells supplied from augmentation solutions with nearly 30% of the retained cells detected within column pore fluids and the remainder attached to soil particle surfaces. Only small variations in retained cells were observed between columns suggesting that similar ureolytic activities and cementation distributions could be achieved. Following augmentation, 10 cementation injections were applied to all columns intended to uniformly cement soils. Fig. 4 presents solution urea concentration measurements obtained in all columns 0-, 2-, 4- and 8-h after cementation injections 1, 5, and 10 from all three sampling ports within each column. As shown, full hydrolysis of the injected urea concentration (250 mM) was achieved in all columns within 8 h after injections. As cementation injections continued, progressive increases in ureolytic activity were observed in all columns with complete hydrolysis achieved within two to four hours during cementation injection 10. Increases in ureolytic activity as cementation injections proceeded were also indicated by reductions in the magnitude of urea concentrations measured immediately after injections.

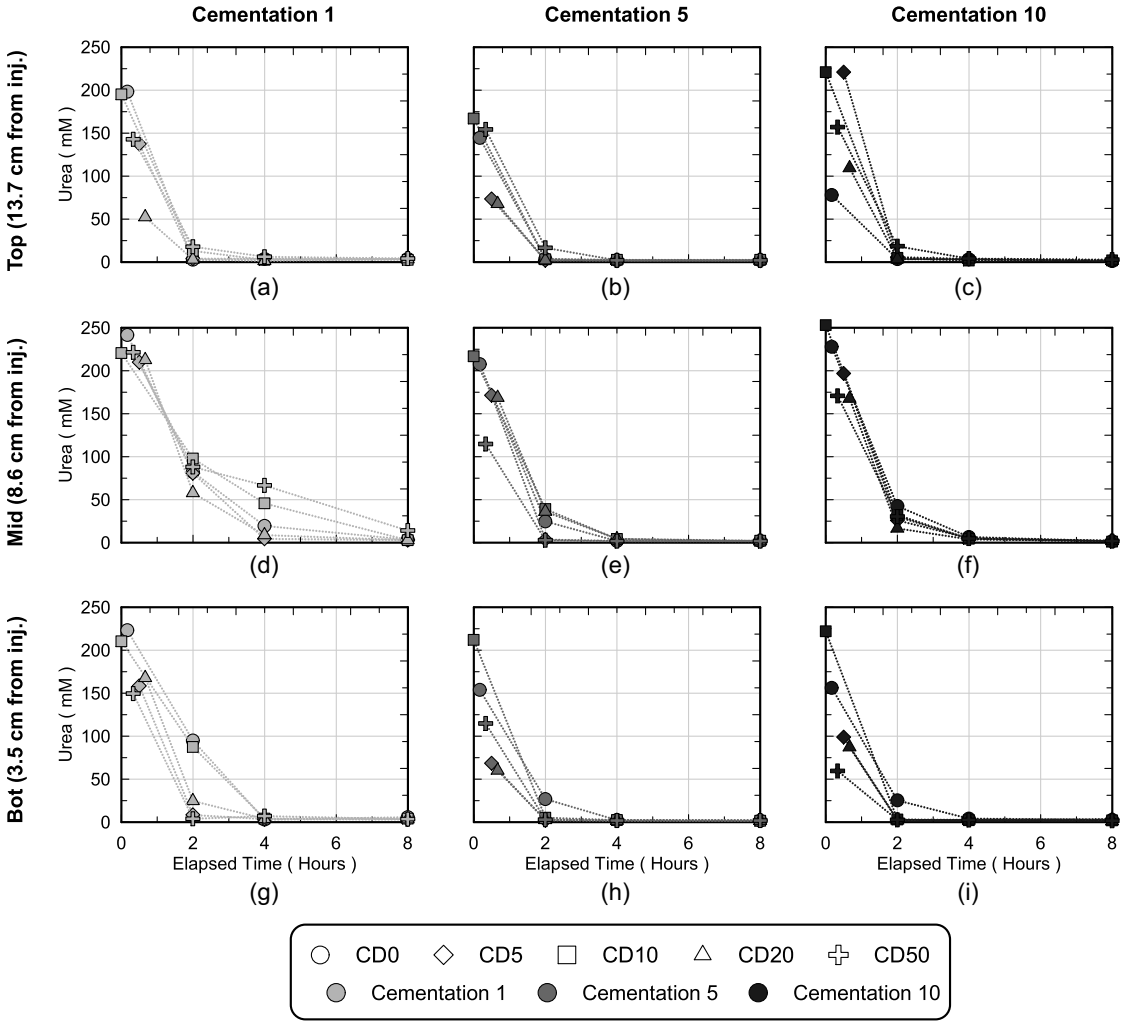

Fig. 4. Urea concentrations in time measured after cementation injection (a, d, and g) 1; (b, e, and h) 5; and (c, f, and i) 10 for all columns at the (a–c) top (13.7 cm from injection); (d–f) middle (8.6 cm from injection); and (g–i) bottom (3.5 cm from injection) sampling port locations.

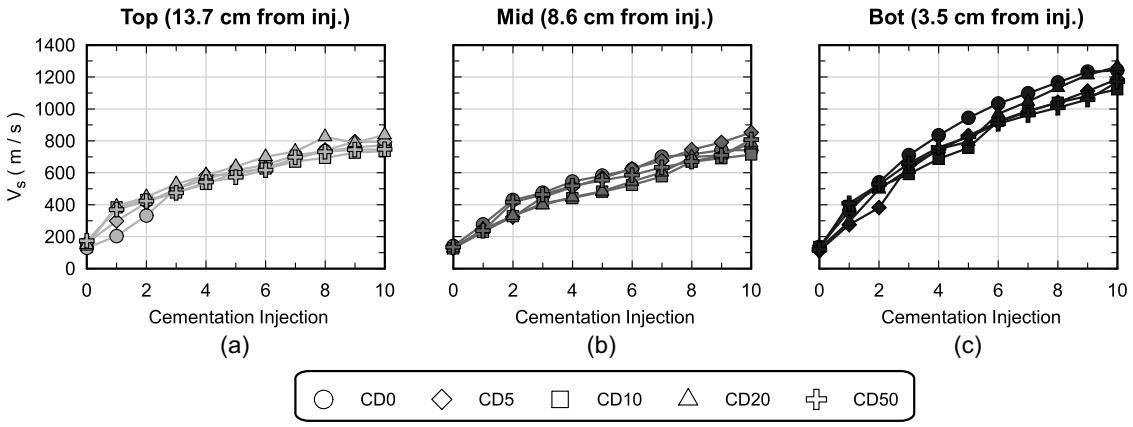

Fig. 5. Soil column shear wave velocity measurements (V_s) obtained from the (a) top (13.7 cm from injection); (b) middle (8.6 cm from injection); and (c) bottom (3.5 cm from injection) locations for all columns versus cementation injection number.

Decreases in initial urea concentrations suggested that increasing and appreciable concentrations of urea were hydrolyzed during injection periods (≈12.5 min) due to accelerating ureolytic activity. When considering ureolytic activity differences spatially within columns, considerably lower activity was measured at the middle sampling port location in all columns during injection 1 when compared to the top and bottom locations. Lower ureolytic activities observed in the middle of columns may have resulted from the augmentation injection strategy wherein cell suspensions were introduced at the top and bottom of columns. For subsequent cementation injections, however, differences in ureolytic activities between locations became less pronounced. When examining aqueous Ca^{2+} concentrations in time (Fig. S1), similar trends were observed with full utilization of the supplied Ca^{2+} achieved in all columns during cementation. Similar ureolytic activities and precipitation rates observed between columns during cementation suggested that differences in cementation magnitudes and distributions were likely minimal. Relationships between urea degradation and $CaCO_3$ precipitation were also examined by comparing aqueous Ca^{2+} and urea concentration measurements obtained at identical times during cementation treatments (Fig. S2). Both urea and Ca^{2+} concentrations were similar in time for all injections and suggested that $CaCO_3$ precipitation occurred rapidly following CO_3^{2-} availability from urea hydrolysis, similar to observations by Burdalski and Gomez (2020).

Measurements of V_s were performed during cementation injections to nondestructively monitor increases in soil small-strain shear stiffnesses indicative of increases in biocementation. Soil V_s has been shown to increase in a near-linear manner with increases in soil $CaCO_3$ contents for poorly graded sands (Martinez et al. 2013; Montoya and DeJong 2015; Lin et al. 2016; Gomez and DeJong 2017; DeJong et al. 2022). Fig. 5 presents V_s values for all columns measured 24 h after cementation injections obtained from the top, middle, and bottom bender element sensors. As shown, initial V_s values ranged between 130 m/s and 174 m/s, 126 m/s and 141 m/s, and 111 m/s and 135 m/s in all columns at the top, middle, and bottom locations, respectively. Although initial V_s distributions were similar between columns, higher V_s values at the top of the columns likely resulted from the vertical stress which was applied using a compliant top cap and the shedding of the applied vertical stress with depth to column sidewalls. During cementation, consistent V_s increases were observed in all columns at similar locations, reflective of comparable increases in biocementation magnitudes following each treatment. After 10 cementation injections, V_s values varied between 736 m/s and 836 m/s (average ΔV_s increase = 625 m/s), 713 m/s and 850 m/s (average ΔV_s increase = 649 m/s), and 1,123 and 1,264 m/s (average ΔV_s increase = 1,072 m/s), at column top, middle, and bottom locations, respectively. While column ΔV_s increases were similar at both the top and middle locations, significantly larger V_s values were observed at the bottom location indicative of greater $CaCO_3$ precipitation. Despite some spatial differences, V_s trends were similar between all columns and varied by less than 10% for similar locations and treatments. Near identical passive tracer behaviors, ureolytic activities, $CaCO_3$ precipitation rates, and V_s trends in time collectively suggested that all columns behaved as near replicates with similar post-treatment $CaCO_3$ content distributions also expected. These similarities allowed for the subsequent study of dissolution progression in nearly identical biocemented columns.

Dissolution Progression in Soil Columns

Following all cementation injections, columns were rinsed to remove reaction by-products and acidic dissolution injections were subsequently applied. Fig. 6 presents V_s measurements obtained 13.7 cm (top), 8.6 cm (middle), and 3.5 cm (bottom) from the injection location in all columns 24 h after all dissolution injections. Measurements of V_s were performed to nondestructively monitor cementation degradation magnitudes and distributions between columns at various times. As shown, measurements were obtained for up to 50 dissolution injections (CD50), with select columns taken offline and destructively sampled after 5 (CD5), 10 (CD10), and 20 (CD20) dissolution injections. Similar V_s trends with applied dissolution injections were observed between all columns with significant spatial changes observed as a function of column length. At the top measurement location, which was furthest from the injection port, V_s values in all columns remained similar during injections reflective of minimal dissolution. In CD50, a ΔV_s reduction of only 29 m/s was observed at this top location after 50 injections. At the middle location, however, average ΔV_s reductions of 82 m/s, 73 m/s, 106 m/s, and 184 m/s, were observed after 5, 10, 20, and 50 injections, respectively. In contrast, V_s measurements at the bottom of columns closest to the injection source exhibited much more dramatic decreases with average ΔV_s reductions of 280 m/s, 300 m/s, 392 m/s, and 826 m/s, observed after 5, 10, 20, and 50 injections, respectively. V_s decreases per injection were largest during the first five dissolution injections at the bottom of columns, after which more gradual V_s reductions were observed. Larger initial V_s reductions may have resulted from the loss of more

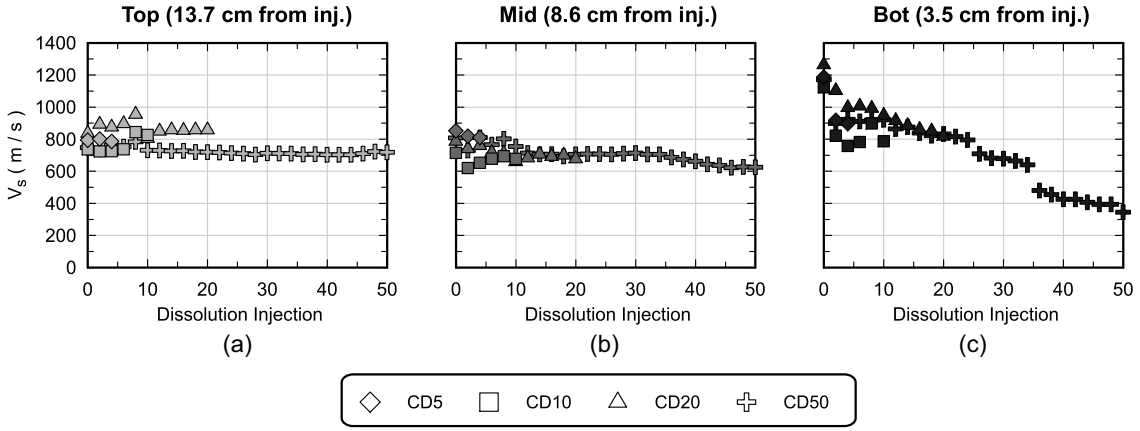

Fig. 6. Soil shear wave velocity measurements (V_s) obtained from the (a) top (13.7 cm from injection); (b) middle (8.6 cm from injection); and (c) bottom (3.5 cm from injection) measurement locations for columns CD5, CD10, CD20, and CD50 versus dissolution injection number.

soluble $CaCO_3$ mineral phases at the start of dissolution injections. Collectively, V_s measurements from all columns suggested that the majority of dissolution was localized near the injection source with minimal dissolution occurring at greater injection distances. Despite injecting solutions at a relatively fast injection rate (1 PV in 12.5 min), $CaCO_3$ dissolution proceeded quickly during the application of acidic solutions, thereby dissolving the greatest magnitudes of $CaCO_3$ near the injection source at the bottom of columns. As solution volumes were transported upwards through columns, solutions quickly approached equilibrium with existing $CaCO_3$ minerals with increases in Ca^{2+} and CO_3^{2-} species and solution pH, thereby resulting in more limited cementation degradation near the top of columns.

Although V_s measurements allowed for indirect assessment of cementation dissolution at specific locations, soil $CaCO_3$ content measurements were also performed following destructive sampling to further characterize changes in $CaCO_3$ content distributions during dissolution. Fig. 7 presents soil $CaCO_3$ content by mass measurements for all columns versus distance from injection location. As shown, immediately after all cementation injections, the $CaCO_3$ content distribution in column CD0 was measured and $CaCO_3$ contents near 4% by mass were observed at most locations with larger values between 5% and 7% observed in the bottom 4 cm as well as elevated values near 5.5% observed near the top of the column. This gradient in cementation was consistent with the observed V_s trends and suggested that higher cementation magnitudes were achieved near the injection source. Slightly higher $CaCO_3$ contents present near the top of this column were not detected by V_s measurements, but likely resulted from the presence of residual solution volumes in the column top cap and effluent tubing. As dissolution injections proceeded, reductions in soil $CaCO_3$ contents occurred. After five dissolution injections (CD5), a $\approx$1% reduction in soil $CaCO_3$ contents was observed immediately adjacent to the injection location (distance = 1 cm); however, at almost all other locations, no detectable dissolution was observed. Following 10 dissolution injections (CD10), more substantial changes in soil $CaCO_3$ contents were observed near the injection location with $CaCO_3$ contents reduced by $\approx$ 4% at a distance of 1 cm when compared to column CD0 with detectable dissolution up to a distance of $\approx$ 5 cm into the column. Similar localization of dissolution within the first 5 cm was observed after 20 injections (CD20) with $CaCO_3$ contents progressively shifting to lower values and the most dramatic reductions again occurring near the injection source. After 50 injections (CD50), more diffuse dissolution was observed, with soil $CaCO_3$ contents approaching 0% over the first 1 cm of column CD50 and detectable dissolution observed up to 10 cm into the column. Measured soil $CaCO_3$ content distributions were consistent with V_s measurements and suggested that the majority of $CaCO_3$ dissolution remained localized near the injection source. $CaCO_3$ content distributions were also integrated with distance along all columns to estimate overall $CaCO_3$ mass losses and suggested that columns had average soil $CaCO_3$ contents of $\approx$ 4.5%, 4.1%, 3.3%, 3.2%, and 1.7% after 0, 5, 10, 20, and 50 dissolution injections, respectively.

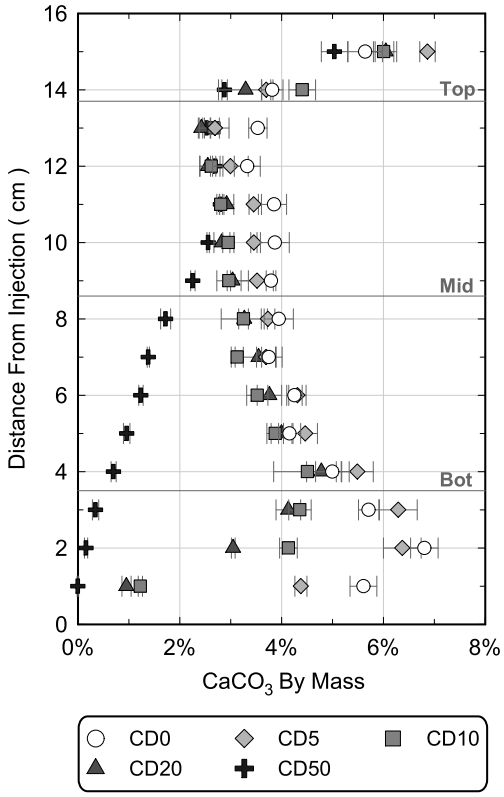

Fig. 7. Soil $CaCO_3$ content by mass measurements versus distance from injection location for all columns. Lines provided indicate the locations of the top, middle, and bottom sampling ports and bender element locations. Provided error bars represent $\pm$ one standard deviation for each measurement obtained from replicates.

Post-Dissolution Microstructural and Mineralogical Differences

Following all dissolution injections, soil subsamples were obtained from the top (12 cm to 14 cm) and bottom (3 cm to 5 cm) of all columns to examine potential changes in biocementation microstructure and mineralogy following dissolution. Fig. 8 presents representative SEM images obtained from columns immediately following cementation (CD0) and after 50 dissolution injections (CD50). As shown, $CaCO_3$ crystals observed in column CD0 immediately following cementation were largely rhombohedral in shape and were consistent with morphologies expected for calcite. After 50 dissolution injections were applied, the spatial density of observed $CaCO_3$ crystals on soil particle surfaces was reduced and crystals appeared to be smaller with less definitive structures. Similar trends were observed for samples obtained after 5, 10, and 20 dissolution injections (CD5, CD10, and CD20) with both crystal sizes and spatial densities decreasing with continued dissolution injections (images not shown). Further testing of the samples was completed using EDS in order to verify the elemental compositions of the observed precipitates given the presence of significant sodium and acetate concentrations in these columns during dissolution (Figs. S3 and S4). EDS analyses suggested that the observed crystals were indeed $CaCO_3$ with only trace amounts of Na^+ detected on the crystals after dissolution injections. XRD analyses were also performed on column subsamples to further examine potential differences in precipitate mineralogy during degradation. While large changes in mineralogy were not expected, it remained unclear if dissolution and subsequent residence periods would alter precipitate mineralogy over progressive dissolution injections. XRD diffraction patterns obtained from subsamples from the top and bottom of columns CD0 and CD50 suggested that calcite was the predominant mineral phase present within precipitates from all samples, with trace amounts of aragonite and vaterite also present. Although no large changes in mineralogical compositions were observed with continued dissolution injections, reductions in calcite masses between CD0 and CD50 samples resulted in reductions in the number of counts for calcite peaks relative to quartz, which was present in the parent soil (Figs. S5 and S6).

Reactive Transport Modeling of Dissolution Progression

Following all soil column experiments, reactive transport numerical modeling was performed to explore the ability of the previously calibrated dissolution kinetic model to capture the spatial and temporal progression of dissolution observed in the physical experiments. Soil $CaCO_3$ content distributions were simulated using dissolution model 1 kinetic parameters ($k_c A_c = 2 \times 10^{-4}$; $n = 14$) that were calibrated using previous batch experiment results (Fig. 2). Fig. 9 presents experimentally measured and modeled soil $CaCO_3$ content distributions following 0, 5, 10, 20, and 50 dissolution injections. As shown in Fig. 9, modeled distributions well approximated experimentally measured values up to 10 dissolution injections, after which simulated values appeared to significantly overpredict dissolution near the injection location. When comparing modeled and measured soil $CaCO_3$ content distributions following 20 dissolution injections (CD20), the model estimated an

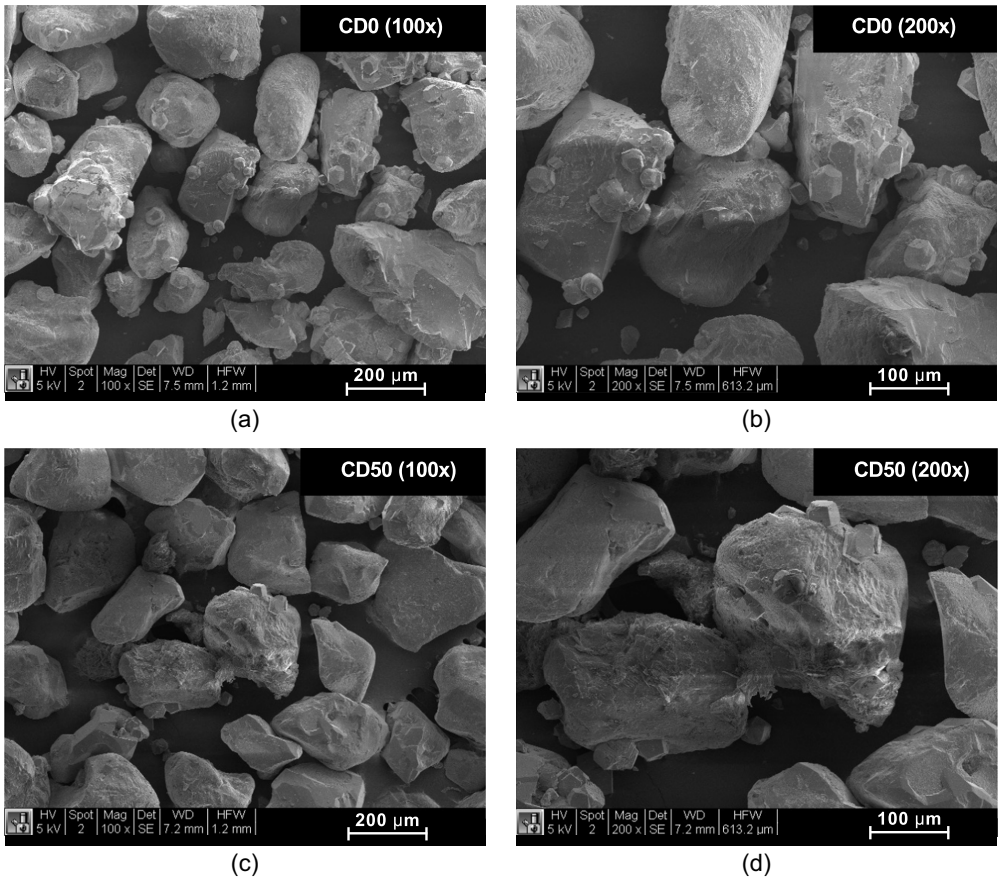

Fig. 8. SEM images of biocemented soil samples obtained from the bottom of columns: (a and b) CD0; and (c and d) CD50 at (a and c) 100×; and (b and d) 200× magnification.

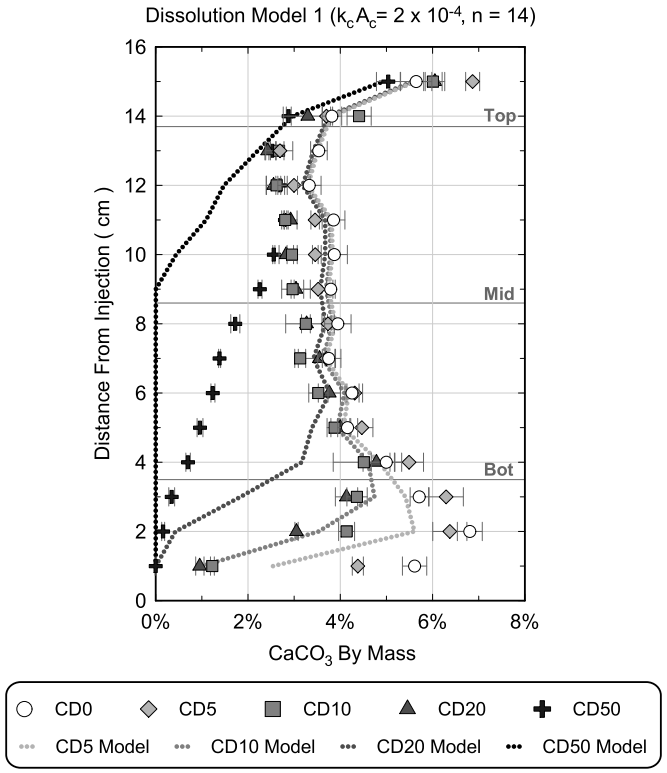

Fig. 9. Comparison between modeled and measured soil $CaCO_3$ contents by mass versus distance from injection location for all columns. Lines indicate the locations of the top, middle, and bottom sampling ports and bender element locations. Modeled values were simulated using dissolution model 1 ($k_cA_c = 2 \times 10^{-4}$ and $n = 14$), which was calibrated to earlier dissolution batch experiments.

average soil $CaCO_3$ content near 1.8% over the first 5 cm, while experimental measurements averaged 3.4% for this same region. The model's overprediction of dissolution magnitudes was even more pronounced when comparing results for 50 dissolution injections (CD50). At this time, the modeled distribution indicated that minimal $CaCO_3$ remained in the first 9 cm of the column; however, experimental measurements showed that much greater $CaCO_3$ contents existed in this region with values exceeding 0.5% at all injection distances greater than 3 cm. Although dissolution model 1 parameters were able to capture changes in aqueous Ca^{2+} concentrations during batch experiments (Fig. 2), these same parameters appeared to significantly overestimate dissolution magnitudes under conditions more representative of in situ soils in the soil column experiments.

In order for simulations to better approximate the dissolution behaviors experimentally observed in soil columns, the dissolution kinetic parameters (k_cA_c and n) were varied to further examine their impact on simulated soil $CaCO_3$ content distributions. Earlier parameter values obtained from batch experiments were shown to overpredict column dissolution magnitudes, therefore further efforts attempted to better calibrate this model to soil column data by altering the dissolution rates via the k_cA_c and n parameters. Fig. 10 presents comparisons between soil $CaCO_3$ content by mass distributions for soil columns simulated using different dissolution model kinetic parameters as well as experimental measurements obtained after cementation (CD0) and after 50 dissolution injections (CD50). Model k_cA_c values were varied from the batch experiment calibrated value of 2×10^{-4} and considered k_cA_c values of 2×10^{-5} [Fig. 10(a)], 4×10^{-5} [Fig. 10(b)], 6×10^{-5} [Fig. 10(c)], and 2×10^{-4} [Fig. 10(d)]. For each k_cA_c value considered, n values were also varied from the batch experiment calibrated value of 14 with simulations for n values of 14, 30, 45, 60, 75, and 90 shown for each discrete k_cA_c value considered. As shown in Fig. 10, variations in k_cA_c values largely controlled the shape of the dissolution distributions, whereas n values largely controlled dissolution magnitudes for a given distribution. These outcomes result from the more significant effect of k_cA_c values on initial dissolution rates occurring during injections and the greater influence of n values on dissolution rates during solution residence periods following injections as equilibrium conditions are approached. Increases in k_cA_c values and decreases in n values both result in faster dissolution rates and therefore greater dissolution near the injection source. In contrast, reductions in k_cA_c values and increases in n values result in reduced dissolution rates, more limited reactions during injections, and therefore more diffuse degradation of cementation along column lengths, albeit with reductions in dissolution magnitudes.

In order to compare the ability of the considered k_cA_c and n value combinations to capture the experimentally observed dissolution trends, relative errors between soil $CaCO_3$ content by mass model estimates and experimental measurements following 50 dissolution injections were determined. Relative errors were computed as the difference between modeled and measured soil $CaCO_3$ contents normalized by the measured values [Eq. (3)]. Fig. 11 presents relative errors (in percent) between modeled and measured soil $CaCO_3$ contents for 50 dissolution injections versus column lengths. When comparing all simulations, relative errors varied between 100% underestimation and 693% overestimation of the measured values at any given location, with the largest errors generally occurring near the injection source wherein the greatest $CaCO_3$ dissolution occurred

$$\text{Relative Error}(\%) = \frac{CaCO_{3\,\text{modeled}} - CaCO_{3\,\text{measured}}}{CaCO_{3\,\text{measured}}} \times 100\% \quad (3)$$

In order to quantitatively assess goodness of fit between modeled estimates and experimental values along column lengths, relative errors were averaged along column lengths for all simulations (Table S1). Simulations using a k_cA_c of 4×10^{-5} and n value of 75 resulted in the smallest average relative error of all considered simulations at 13%, which was a significant improvement when compared to the batch experiment calibrated dissolution model 1 parameters ($k_cA_c = 2 \times 10^{-5}$ and $n = 14$), which had an average relative error of 67%. In contrast, simulations assuming a k_cA_c of 2×10^{-5} and n value of 90 had the highest average relative error of the considered combinations at 79%. Although not shown, similar relative error calculations were also performed for 5, 10, and 20 dissolution injections for which simulations assuming a k_cA_c of 4×10^{-5} and n value of 75 again exhibited improved fits over the other considered parameter combinations. Although these k_cA_c and n parameters could likely have been further refined to better match the experimental data, further parameter optimizations were avoided to mitigate potential overfitting of the model to the experimental dataset. Following these findings, these kinetic parameters ($k_cA_c = 4 \times 10^{-5}$, $n = 75$) were referred to as dissolution model 2 parameters and results simulated using these values were compared to those obtained from dissolution model 1. Fig. 12 provides a comparison between soil $CaCO_3$ contents by mass estimated using the refined dissolution model 2 parameters ($k_cA_c = 4 \times 10^{-5}$ and $n = 75$) and experimental soil $CaCO_3$ content data from columns CD0, CD5, CD10, CD20, and CD50. Although small differences in measured soil column $CaCO_3$ contents were observed for dissolution injections 5 and 10, at further times wherein more substantial

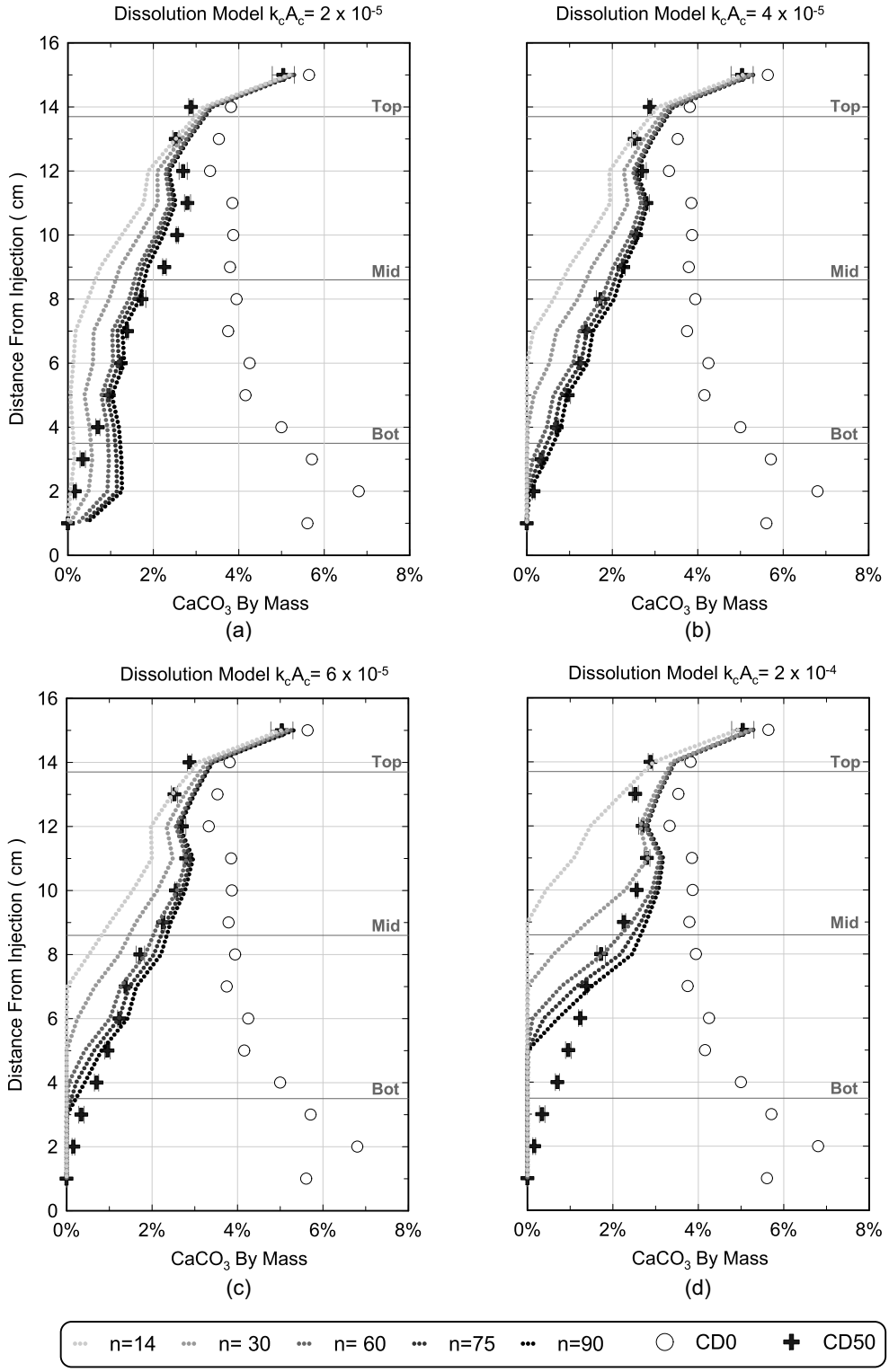

Fig. 10. Comparisons between soil $CaCO_3$ content by mass distributions simulated using different dissolution model kinetic parameters (k_cA_c and n) and experimental measurements obtained after cementation (CD0) and after 50 dissolution injections (CD50). Plots present simulated values for (a) $k_cA_c = 2 \times 10^{-5}$; (b) $k_cA_c = 4 \times 10^{-5}$; (c) $k_cA_c = 6 \times 10^{-5}$; and (d) $k_cA_c = 2 \times 10^{-4}$ for n values of 14, 30, 60, 75, and 90.

$CaCO_3$ contents changes were observed (i.e., dissolution injections 20 and 50), dissolution model 2 simulated values were able to closely capture experimental trends along all columns with length.

While the previously examined dissolution model 1 and 2 parameter sets achieved varying degrees of success with respect to capturing soil $CaCO_3$ content distributions during dissolution injections, the ability of these models to capture aqueous chemical changes during dissolution was not yet evaluated. Fig. 13 presents aqueous Ca^{2+} concentration measurements obtained from all sampling ports immediately after injections (0 h) and after 24-h solution retention periods during dissolution injections 10, 20 and 50 for columns CD10, CD20, and CD50 along with simulated Ca^{2+}

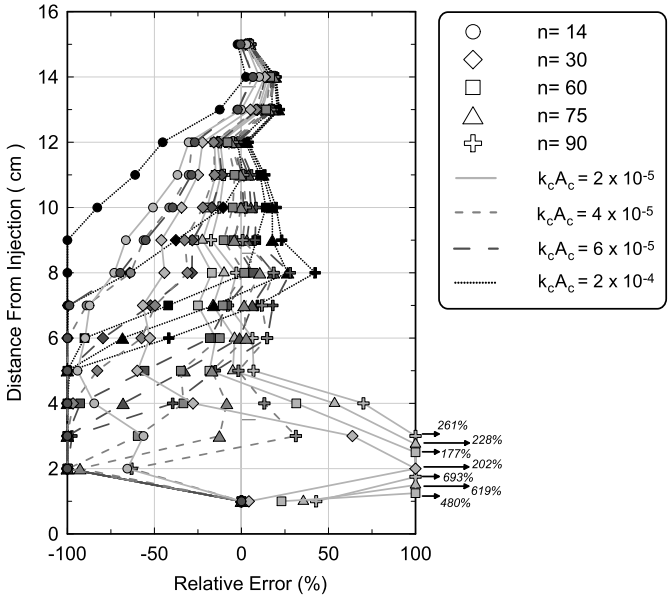

Fig. 11. Comparison of soil $CaCO_3$ content by mass relative model errors for all k_cA_c and n value-varied simulations as a function of column length. All modeled values and measurements (from CD50) were compared for 50 dissolution injections. Models considered k_cA_c values of 2×10^{-5}, 4×10^{-5}, 6×10^{-5}, and 2×10^{-4} as well as n values of 14, 30, 60, 75, and 90.

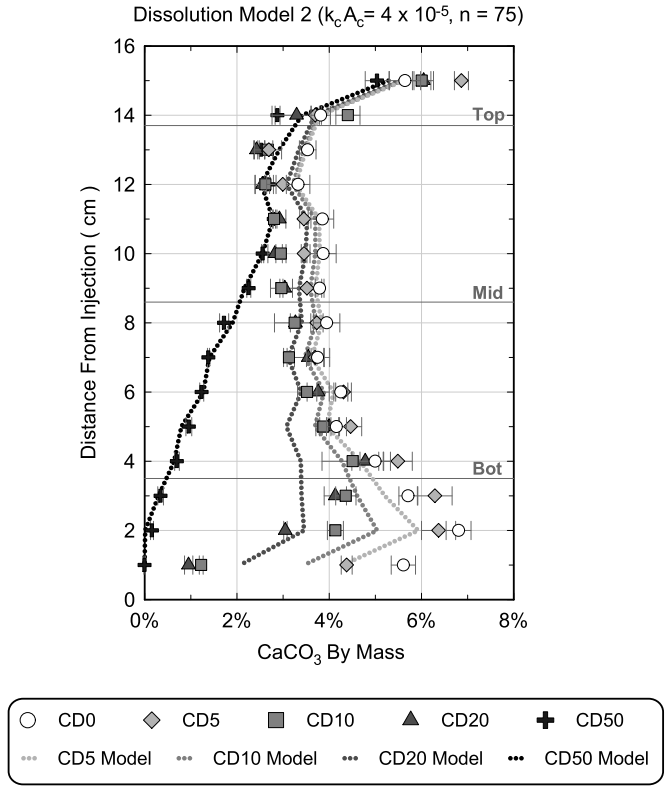

Fig. 12. Comparison between modeled and measured soil $CaCO_3$ contents by mass versus distance from injection location for all columns. Lines indicate the locations of the top, middle, and bottom sampling ports and bender element locations. Modeled values were simulated using dissolution model 2 ($k_cA_c = 4 \times 10^{-5}$ and $n = 75$) parameters, which were shown to minimize relative errors between modeled and measured $CaCO_3$ content values.

concentrations obtained from dissolution models 1 and 2. As shown for both dissolution injections 10 and 20, aqueous Ca^{2+} concentrations measured immediately after injections varied between 20 and 30 mM at all locations with 24-h measurements exhibiting only slightly elevated values between 25 and 32 mM. Similar concentrations measured immediately after injections and after the 24-h residence periods indicated that $CaCO_3$ dissolution occurred rapidly during injections with minimal changes occurring during residence periods. When comparing simulated Ca^{2+} concentrations from dissolution models 1 and 2, similar trends were observed with a gradient in values anticipated by both models immediately after injections, but more uniform Ca^{2+} concentrations expected at all locations 24 h after injections. For both time periods, experimentally measured Ca^{2+} concentrations were better approximated by dissolution model 1, with dissolution model 2 underestimating Ca^{2+} concentrations. For later injections, dissolution model 1 predicted that Ca^{2+} concentrations would be near zero immediately adjacent to the injection source 24 h after dissolution injection 10, reflective of the complete dissolution and absence of $CaCO_3$ expected in this region. In contrast, dissolution model 2 simulated that Ca^{2+} concentrations remained uniform across columns but were lower in magnitude indicating that sufficient $CaCO_3$ remained. For dissolution injection 50, both models predicted significant gradients in both post-injection and 24-h Ca^{2+} concentrations due to more limited $CaCO_3$ remaining near the injection source. Although dissolution model 2 better approximated measured Ca^{2+} concentrations between 0 mM and 20 mM after injection, interestingly, dissolution model 1 again achieved improved predictions of 24-h Ca^{2+} concentrations with values near 0 mM expected at the bottom sampling location wherein $CaCO_3$ was depleted and higher Ca^{2+} concentrations near 25 mM expected at the middle and top sampling locations. Collectively, these results suggested that while dissolution model 2 parameters achieved improved estimates of soil $CaCO_3$ content distributions during dissolution injections, dissolution model 1 parameters afforded improved predictions of aqueous Ca^{2+} concentrations.

In order to further examine the ability of the considered models to track cumulative $CaCO_3$ mass losses during dissolution injections, effluent solutions were collected and homogenized from all column experiments during select dissolution injections and bulk effluent Ca^{2+} concentrations and pH values were measured. Bulk effluent solution measurements allowed for the estimation of the mass of $CaCO_3$ dissolved each injection, which could then be compared to estimates from earlier soil $CaCO_3$ content measurements. Fig. 14 presents both measured bulk effluent Ca^{2+} concentrations [Fig. 14(a)] and solution pH values [Fig. 14(b)] versus dissolution injection number as well as simulated values using dissolution model 1 and 2 parameters. As shown in Fig. 14(a), measured effluent Ca^{2+} concentrations exiting columns during injection 1 were near 0 mM reflective of the deionized water present initially within columns being largely displaced by injected dissolution solutions. For all further injections, however, effluent Ca^{2+} concentrations ranged between $\approx$ 4 to 7 mM with most values between $\approx$ 5 and 6 mM. Although similar for all injections, effluent Ca^{2+} concentrations slightly decreased during later dissolution injections, reflective of the absence of dissolution at some locations near the injection source wherein $CaCO_3$ was depleted. When comparing simulated effluent values, trends similar to those measured spatially within columns (Fig. 13) were observed with higher effluent Ca^{2+} concentrations predicted by dissolution model 1 parameters than dissolution model 2. Both models also indicated slight decreases in effluent Ca^{2+} concentrations with continued dissolution injections, as expected. Although both models predicted values that were

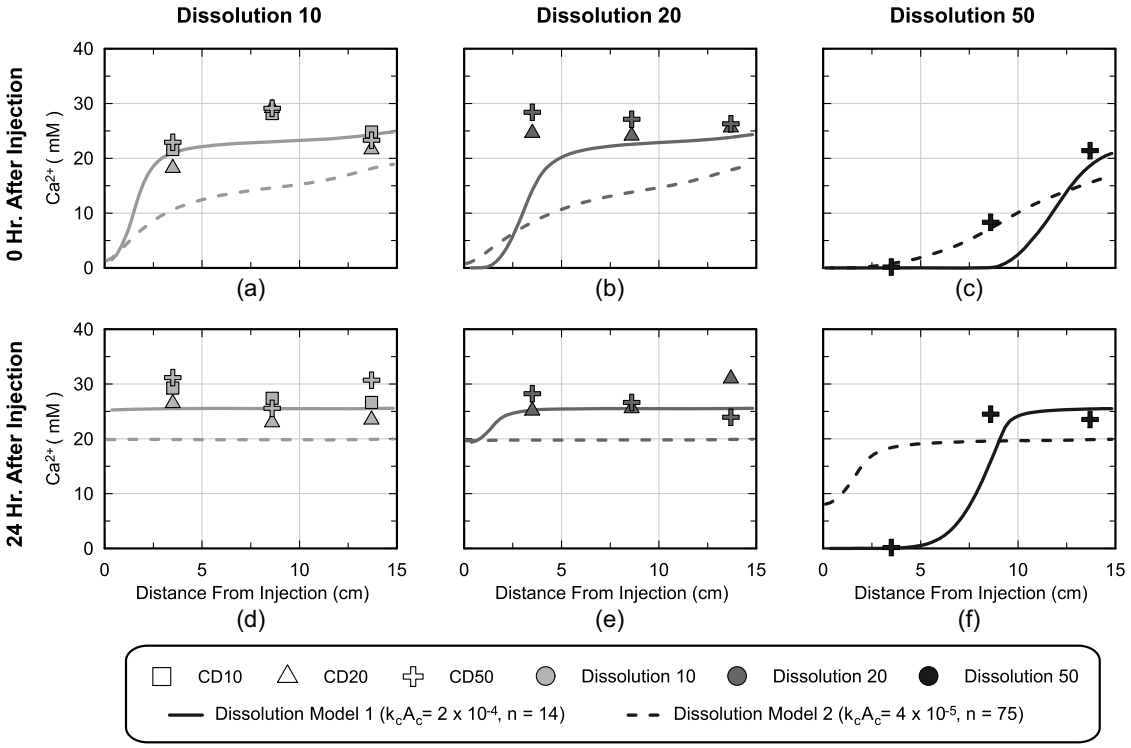

Fig. 13. Comparison of modeled and measured aqueous Ca^{2+} concentration measurements versus distance from injection source from top, middle, and bottom sampling ports immediately after (0 h) and 24 h after dissolution injection (a and d) 10; (b and e) 20; and (c and f) and 50 obtained from columns CD10, CD20, and CD50. Modeled values were obtained from simulations using dissolution model 1 ($k_cA_c = 2 \times 10^{-4}$ and $n = 14$) and 2 ($k_cA_c = 4 \times 10^{-5}$ and $n = 75$) parameters.

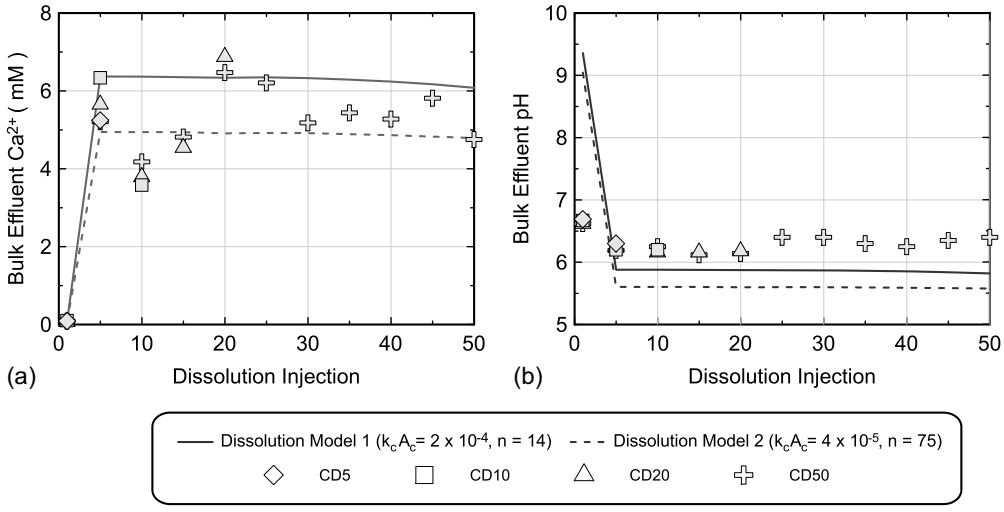

Fig. 14. Comparison of modeled and measured (a) bulk effluent Ca^{2+} concentrations; and (b) pH values obtained from columns CD5, CD10, CD20, and CD50 versus dissolution injection number. Modeled results were obtained from simulations with dissolution model 1 ($k_cA_c = 2 \times 10^{-4}$ and $n = 14$) and 2 ($k_cA_c = 4 \times 10^{-5}$ and $n = 75$) parameters.

within the scatter of experimental measurements, dissolution model 2 appeared to follow experimental trends most closely. When comparing effluent pH trends as shown in Fig. 14(b), experimental measurements suggested near constant pH values between ≈ 6 and 6.5 for all dissolution injections; however, both dissolution models underpredicted these values. Similar underprediction of pH values was also observed during batch experiments, wherein modeled values were significantly smaller (Fig. 2). It should be mentioned, however, that simulated pH values significantly overpredicted experimental pH values at the transition to dissolution injections (injection 1) during which residual solution species present within columns significantly altered pH values.

Although the ability of dissolution model 1 and 2 parameters to capture changes in solution chemistry and soil $CaCO_3$ content distributions was examined, it remained unclear if these models could similarly capture changes in bulk masses of $CaCO_3$ lost and if such

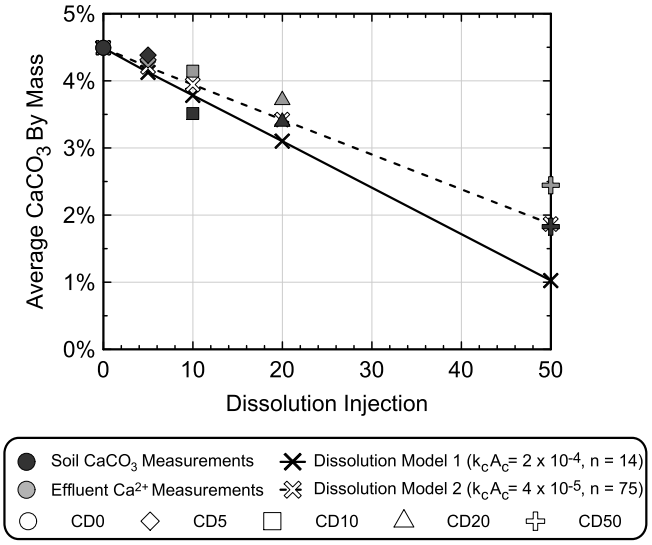

Fig. 15. Comparison of average soil column $CaCO_3$ contents by mass versus dissolution injections determined from soil $CaCO_3$ content measurements, effluent Ca^{2+} concentration measurements, and simulated soil $CaCO_3$ contents. Modeled results were obtained from simulations with dissolution model 1 ($k_cA_c = 2 \times 10^{-4}$ and $n = 14$) and 2 ($k_cA_c = 4 \times 10^{-5}$ and $n = 75$) parameters.

predictions would compare favorably to $CaCO_3$ mass losses estimated from both measured soil $CaCO_3$ contents and effluent Ca^{2+} concentrations. Fig. 15 presents average soil $CaCO_3$ contents by mass determined experimentally using measured soil $CaCO_3$ contents and bulk effluent Ca^{2+} concentrations as well as simulated average soil $CaCO_3$ contents determined from dissolution model 1 and 2 parameters versus dissolution injection number. The presented experimental values were determined by either (1) integrating measured soil $CaCO_3$ contents along column lengths; or (2) estimating masses of $CaCO_3$ lost during dissolution injections from measured bulk effluent Ca^{2+} concentrations and injected volumes and assuming an initial average $CaCO_3$ content identical to CD0 measured directly after cementation. As shown, experimental values determined from both soil $CaCO_3$ contents and bulk effluent Ca^{2+} concentrations were consistent, with an average $CaCO_3$ content near 4.5% measured initially and average $CaCO_3$ contents between 2% and 2.5% by mass after 50 dissolution injections. Although aqueous measurements alone could not provide insights regarding the distribution of cementation degradation, such measurements may provide a metric by which the magnitudes of cementation degradation can be monitored at field sites, provided that groundwater gradients and volume fluxes are also measured. When comparing measured and simulated values, dissolution model 2 better approximated the experimental data with dissolution model 1 again significantly overestimating dissolution magnitudes in time.

Dissolution Model and Experimental Comparisons

Differences in dissolution kinetic model parameters yielded significant impacts with respect to simulated soil $CaCO_3$ content distributions and aqueous chemical changes and accordingly achieved varying degrees of consistency with measurements from the physical soil column experiments. Kinetic parameters employed in dissolution model 1 were calibrated to independent batch experiments to enable prediction of Ca^{2+} concentration changes in time indicative of $CaCO_3$ dissolution. Although dissolution model 1 was able to accurately simulate aqueous Ca^{2+} concentrations observed within columns during the dissolution process, this model significantly overestimated the magnitudes of soil $CaCO_3$ dissolution. Acknowledging these limitations, kinetic parameters were further modified to better approximate the spatial and temporal changes in soil $CaCO_3$ contents measured directly from soil columns. A k_cA_c value of 4×10^{-5} and n value of 75 were used in dissolution model 2 and were shown to closely reproduce changes in soil $CaCO_3$ content distributions and cumulative $CaCO_3$ mass losses during dissolution injections. The inability of dissolution model 1 to accurately predict experimental soil $CaCO_3$ content changes during dissolution may have resulted from a variety of reasons: (1) Dissolution model 1 parameters were calibrated solely to predict changes in aqueous Ca^{2+} concentrations observed during batch experiments. Accordingly, the model was able to reasonably capture aqueous chemical changes in column experiments, but predictions of soil $CaCO_3$ contents were less successful. (2) Dissolution batch experiments were continuously agitated and aimed to capture the dissolution kinetics of biocementation under homogenous solution conditions. As a result, such experiments could not fully capture the more complex geochemical conditions experienced during advective-dispersive transport of dissolution solutions through soil columns. Additional complexities resulting from advective-dispersive transport may include differences in the exposure time of $CaCO_3$ surfaces to dissolution solutions as well as localized differences in geochemical conditions due to solution dispersion and stop-flow retention periods. (3) A one-dimensional reactive transport model was used to predict soil $CaCO_3$ content distributions. This model assumed homogenous 1D flow and inherently could not fully account for potential localization of dissolution within the porous media. Although breakthrough curves obtained before and after biocementation suggested that minimal differences in transport conditions resulted from the process, increased dissolution may have occurred along preferential flow paths which could have formed during the dissolution process, thereby allowing for other regions to remain more heavily cemented. Spatial differences in soil $CaCO_3$ contents were evaluated along column lengths, but such measurements could not resolve smaller scale differences across sample cross-sections due to measurement sample size requirements. Although not definitive, visual observations during destructive sampling of columns suggested that some more heavily dissolved flow paths may have existed within columns. If such localization occurred, both more heavily cemented locations and more heavily dissolved locations would be homogenized prior to soil $CaCO_3$ content measurements and could have resulted in elevated $CaCO_3$ contents when compared to those predicted by dissolution model 1. This discrepancy between the models and physical soil column experiments may explain why dissolution model 1 was able to more accurately capture aqueous Ca^{2+} concentrations in time, representative of pore fluids reaching equilibrium with $CaCO_3$, while significantly underpredicting measured soil $CaCO_3$ contents for section subsamples. (4) Lastly, it also remains possible that dissolution rates may have slowed over time due to the progressive weathering of mineral surfaces. Although all models assumed constant k_cA_c and n kinetic parameters during the dissolution process, previous studies examining the dissolution of carbonate minerals have shown that such parameters may change over time due to the modification of reactive surface areas during dissolution, which can act to progressively slow dissolution rates (Morse and Arvidson 2002).

Although discrepancies in the predictive capabilities of the considered dissolution models were observed, the obtained results suggest that existing dissolution kinetic frameworks can be used successfully to predict the dissolution behavior of biocemented soils under conditions representative of in situ soils. However, when

developing such models, independent calibration experiments may be needed which maintain greater parity between the conditions present during calibration and those for which model predictions are desired. For example, if the primary goal is to analyze changes in soil engineering characteristics over time as captured by changes in soil $CaCO_3$ contents, calibration of model parameters to soil $CaCO_3$ content measurements from soil column experiments may be needed. However, if instead the primary goal is to predict aqueous geochemical trends, calibration of dissolution kinetic model parameters to batch experiments may be acceptable. While the explored kinetic parameter sets allowed for experimental observations to be well-captured in this study, further research is needed to better understand how these kinetic model parameters may vary as a function of solution chemistry, transport conditions, and biocementation characteristics in order to more fully understand the utility of such models for prediction of biocementation permanence under different conditions.

$CaCO_3$ *Content and* V_s *Relationships during Dissolution*

Numerous researchers have shown the ability of V_s measurements to track changes in soil $CaCO_3$ contents during biocementation (Gomez et al. 2017); however, how such relationships may shift during cementation degradation has remained unexplored. Previous studies have shown that differences in the interparticle spatial distribution of cementation can influence V_s increases during cementation (Lin et al. 2020) and therefore it was expected that the interparticle distribution of dissolution (i.e., on particle contacts versus open surfaces) may impact how these relationships would evolve during degradation. Fig. 16 presents soil V_s values versus soil $CaCO_3$ contents measured at top, middle, and bottom locations during both cementation and dissolution treatments for column CD50. Although soil column V_s values were measured daily during cementation and dissolution injections, soil $CaCO_3$ content measurements were only obtained on select days when columns were destructively sampled. Since V_s and $CaCO_3$ content values were measured for CD0 after cementation, a linear relationship between V_s and $CaCO_3$ content values was assumed during cementation in order to estimate changes in $CaCO_3$ contents with changes in V_s. However, in order to estimate changes in soil $CaCO_3$ contents during dissolution injections, dissolution model 2 predictions, which were shown to reasonably capture cementation distributions in time, were used for all days for which $CaCO_3$ contents were not directly measured, with direct measurements used where possible. As shown in Fig. 16, minimal dissolution was observed at the top measurement location, but greater dissolution was observed at both the middle and bottom locations with some differences in the relationships between V_s and soil $CaCO_3$ contents apparent between the dissolution and cementation phases. In general, slightly higher V_s values were observed for the same $CaCO_3$ content during dissolution when compared to cementation. The higher V_s values observed for the same $CaCO_3$ content during dissolution may reflect greater dissolution of $CaCO_3$ on soil particle surfaces with greater retention of cementation at particle contacts thereby maintaining shear stiffness enhancements. The relatively fast rate of dissolution observed and the greater flow velocities expected through open soil pores as opposed to more stagnant zones near particle contacts (Minto et al. 2019) may have promoted $CaCO_3$ dissolution on particle surfaces with more minimal dissolution occurring at contacts.

Fig. 17 presents changes in shear wave velocities (ΔV_s) versus changes in soil $CaCO_3$ contents ($\Delta CaCO_3$) for all columns during cementation and dissolution injections. As shown, relationships during cementation injections were similar between all locations and columns with ΔV_s increases between 125 m/s and 190 m/s observed for $\Delta CaCO_3$ increases of 1% by mass. At the top measurement location, limited dissolution was observed in all columns; however, as expected, more significant ΔV_s decreases were observed at the middle and bottom measurement locations. When comparing relationships during dissolution and cementation, significant differences in ΔV_s and $\Delta CaCO_3$ slopes were observed. For example, for the middle measurement location, a $\Delta CaCO_3$ reduction during dissolution of 2% by mass corresponded to a ΔV_s decrease near 120 m/s, while during cementation a similar 2% calcite content increase corresponded to a significantly larger ΔV_s increase near 340 m/s. Similar trends were also observed for the bottom measurement location with $\Delta CaCO_3$ reductions during dissolution again having a more limited effect on ΔV_s when compared to cementation. Although differences in the mechanisms of dissolution versus precipitation were hypothesized, future investigations examining changes in cementation microstructures during the dissolution process may provide further insights regarding differences in the observed ΔV_s and $\Delta CaCO_3$ relationships. Improved understandings of such relationships will likely prove critical towards enabling in situ assessment of biocementation integrity following field applications. Ultimately, further mechanical testing may also

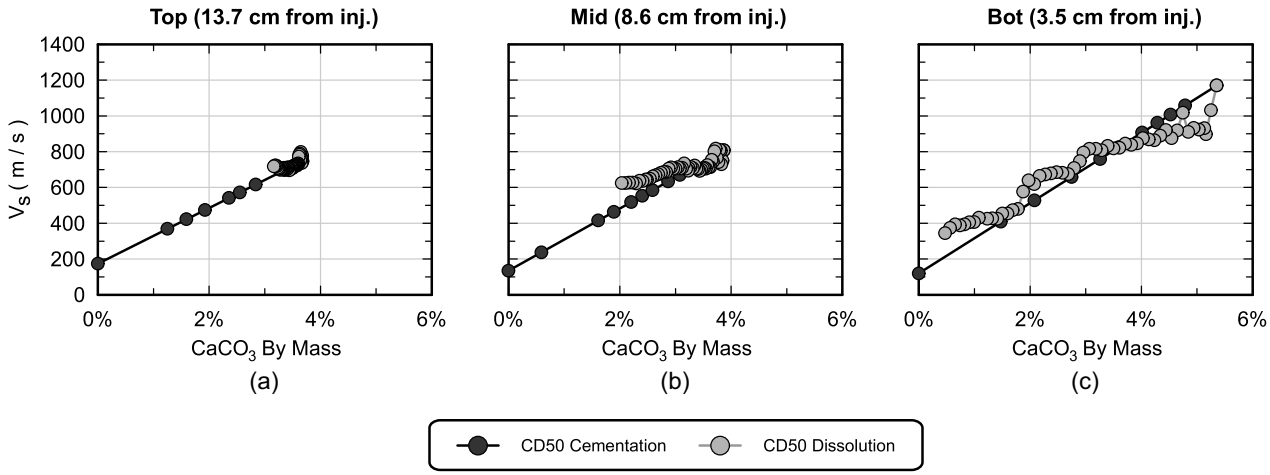

Fig. 16. Soil shear wave velocities (V_s) versus soil $CaCO_3$ content by mass measurements obtained from column CD50 at the (a) top (13.7 cm from injection); (b) middle (8.6 cm from injection); and (c) bottom (3.5 cm from injection) locations during both cementation and dissolution injections.

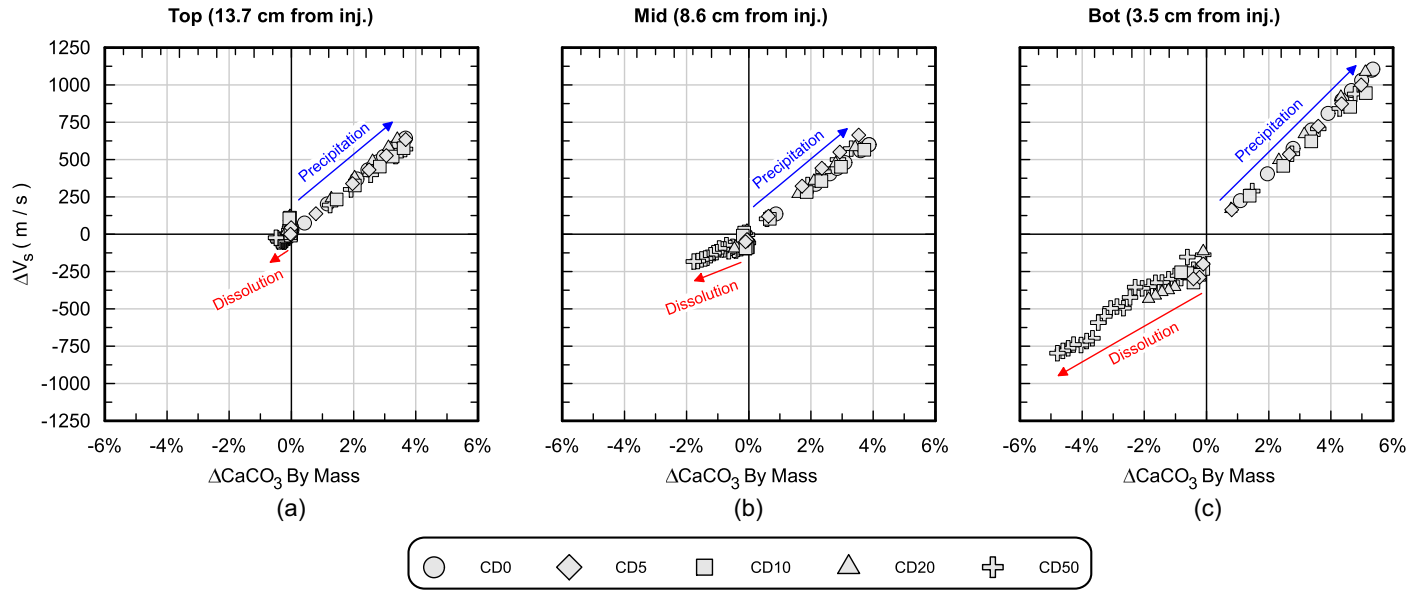

Fig. 17. Changes in soil shear wave velocities (ΔV_s) versus changes in $CaCO_3$ content by mass ($\Delta CaCO_3$) obtained from all columns at (a) top (13.7 cm from injection); (b) middle (8.6 cm from injection); and (c) bottom (3.5 cm from injection) locations during cementation and dissolution treatments.

be necessary to understand how engineering behaviors of interest may shift as a function of decreases in soil $CaCO_3$ content magnitudes, ΔV_s reductions, as well as dissolution and cementation past history.

Conclusions

A study was performed to investigate the dissolution behavior of ureolytic biocementation using batch reaction and soil column experiments in conjunction with reactive transport numerical modeling. Two dissolution batch experiments were first performed wherein biocemented sands were subjected to acidic dissolution solutions and aqueous Ca^{2+} concentrations were monitored in time indicative of $CaCO_3$ dissolution. A dissolution kinetic model was used to simulate observed dissolution during batch experiments and the kinetic parameters k_cA_c and n were calibrated to match the experimental data. Following calibration to batch experiments, a soil column experiment was performed to examine biocementation dissolution under conditions more representative of in situ soils in order to assess the ability of the previously calibrated model to forward predict dissolution behaviors. Five soil columns received 10 identical daily biocementation injections and achieved relatively uniform soil $CaCO_3$ contents near 5% by mass. Following biocementation, columns received either 0, 5, 10, 20, or 50 daily acidic dissolution solution injections and the spatial and temporal progression of $CaCO_3$ dissolution were examined at various points in time using V_s, aqueous Ca^{2+} concentration, pH, and XRD measurements as well as SEM imaging. Model predictions and experimental results were then compared, and dissolution kinetic parameters were further modified to better capture experimental behaviors from columns.

From the results of this study, the following conclusions can be made:

- Experimental observations from both batch and soil column experiments demonstrated that $CaCO_3$ dissolution occurs quickly upon the introduction of acidic undersaturated solutions. In soil column experiments, this fast rate of dissolution resulted in significant degradation of biocementation near the injection location with more minimal dissolution observed at greater injection distances. This was particularly noteworthy given the relatively fast injection rates employed (0.08 pore volumes per minute). Although site-specific differences in surrounding soil solution chemistries will further alter dissolution rates experienced at various field locations, these results suggest that the majority of dissolution may occur near the perimeter of biocemented soil zones, with solutions rapidly equilibrating with $CaCO_3$ minerals during transport, thereby limiting $CaCO_3$ dissolution at greater distances within treated regions.
- Existing dissolution kinetic models for $CaCO_3$ were shown to reasonably predict the dissolution behavior of ureolytic biocementation under both batch reaction and one-dimensional transport conditions; however, modification of k_cA_c and n parameters were needed. Although dissolution model 1 parameters were able to accurately simulate aqueous Ca^{2+} concentration measurements in time from both batch and soil column experiments, this same model significantly overpredicted magnitudes of dissolution as measured by soil column $CaCO_3$ content distributions and bulk effluent Ca^{2+} concentrations.
- When k_cA_c and n parameters were varied, large changes in simulated $CaCO_3$ content distributions were observed with k_cA_c values largely controlling the shape of the dissolution distributions and n values primarily controlling the magnitudes of dissolution. Dissolution model 2 parameters, which had a decreased k_cA_c and increased n value relative to model 1, allowed for reductions in simulated dissolution rates and an improved fit to soil column data. Although additional verification of this model remains needed to demonstrate its utility across a broader range of geochemical conditions, the obtained results suggest that calibration of dissolution kinetic models to soil column $CaCO_3$ content data may be required in order to enable accurate prediction of soil $CaCO_3$ content changes during dissolution. Furthermore, prediction of changes in soil $CaCO_3$ contents may prove critical towards predicting the engineering behaviors of degraded

biocemented materials and should likely be prioritized over prediction of aqueous Ca^{2+} concentrations.

- Although k_cA_c dissolution kinetic parameter values used in this study ($k_cA_c = 4 \times 10^{-5}$ or 2×10^{-4}) compared favorably with those determined by Ribeiro and Gomez (2022) for similar batch experiments involving different acidic solutions ($k_cA_c = 6 \times 10^{-5}$ to 2×10^{-4}), the n value used in dissolution model 2 ($n = 75$) was significantly higher than previous batch experiments ($n = 14$). This may have resulted from the significant differences in dissolution behaviors during one-dimensional reactive transport when compared to batch conditions as well as other differences between the primary datasets used for model calibration.
- Differences in the observed relationships between V_s and soil $CaCO_3$ content changes were observed between dissolution and precipitation events in soil columns, with biocemented soils generally exhibiting larger V_s values for the same $CaCO_3$ content during dissolution versus precipitation. This outcome may have resulted from differences in the interparticle spatial distribution of cementation dissolution when compared to precipitation. It was hypothesized that dissolution may have preferentially degraded cementation on free particle surfaces as opposed to particle contacts due to greater flow velocities experienced by open soil pores and the fast rate of dissolution.

Results from this study significantly improve our understanding of the dissolution kinetics of biocementation and its resulting effects on soil mechanical properties. Future investigations remain needed, however, to demonstrate the efficacy of these model frameworks towards enabling forward prediction of biocementation dissolution under conditions not previously examined as well as to better understand the geotechnical behaviors of biocemented soils following chemical degradation. Such insights regarding the long-term performance of biocementation will likely prove critical towards improving industrial acceptance and confidence in ureolytic biocementation as a geotechnical soil improvement technology.

Data Availability Statement

Some or all data, models, or code that support the findings of this study are available from the corresponding author upon reasonable request. All data presented in the figures of this paper as well as experimental measurements is available through the NSF DesignSafe-CI Data Depot repository (https://www.designsafe-ci.org/data/browser/public/) under Project No. PRJ-3190.

Acknowledgments

Funding for this research work was provided by the National Science Foundation (ECI-1824647) and is greatly appreciated. Research collaboration made possible through the National Science Foundation under NSF Cooperative Agreement No. EEC-1449501 is also acknowledged. Any opinions, findings, and conclusions or recommendations expressed in this manuscript are those of the authors and do not necessarily reflect the views of the National Science Foundation.

Supplemental Materials

Table S1 and Figs. S1–S6 are available online in the ASCE Library (www.ascelibrary.org).

References

Almajed, A. A. 2017. "Enzyme induced carbonate precipitation (EICP) for soil improvement." Ph.D. thesis, School of Sustainable Engineering and the Built Environment, Arizona State Univ.

Al Qabany, A., and K. Soga. 2014. "Effect of chemical treatment used in MICP on engineering properties of cemented soils." In *Proc., Bio- and Chemo-Mechanical Processes in Geotechnical Engineering: Géotechnique Symp. in Print 2013*, 107–115. London: ICE Publishing.

APHA (American Public Health Association). 2005. *Standard methods for the examination of water and wastewater.* 19th ed. Washington, DC: APHA.

ASTM. 2014. *Standard test method for rapid determination of carbonate content of soils*. ASTM D4373-14. West Conshohocken, PA: ASTM.

ASTM. 2016a. *Standard test methods for maximum index density and unit weight of soils using a vibratory table*. ASTM D4253-16e1. West Conshohocken, PA: ASTM.

ASTM. 2016b. *Standard test methods for minimum index density and unit weight of soils and calculation of relative density.* ASTM D4254-16. West Conshohocken, PA: ASTM.

ASTM. 2017. *Standard practice for classification of soils for engineering purpose*. ASTM D2487-17e1. West Conshohocken, PA: ASTM.

Baek, S. H., T. H. Kwon, and J. DeJong. 2022. "Impact of microbially induced calcite precipitation (MICP) on hydraulic conductivity of coarse sands." In *Proc., 20th Int. Conf. on Soil Mechanics and Geotechnical Engineering*. London: International Society for Soil Mechanics and Geotechnical Engineering.

Burbank, M., T. Weaver, T. Green, B. Williams, and R. Crawford. 2011. "Precipitation of calcite by indigenous microorganisms to strengthen liquefiable soils." *Geomicrobiol. J.* 28 (4): 301–312. https://doi.org/10.1080/01490451.2010.499929.

Burdalski, R. J., II. 2020. "Investigating the effect of biological and chemical factors on the reaction kinetics and mineralogy of ureolytic biocementation." Master's thesis, Dept. of Civil and Environmental Engineering, Univ. of Washington.

Burdalski, R. J., and M. G. Gomez. 2020. "Investigating the effect of microbial activity and chemical concentrations on the mineralogy and morphology of ureolytic bio-cementation." In *Geo-Congress 2020: Biogeotechnics*, Geotechnical Special Publication 320, edited by E. Kavazanjian Jr., J. P. Hambleton, R. Makhnenko, and A. S. Budge, 83–95. Reston, VA: ASCE.

Burdalski, R. J., B. G. O. Ribeiro, M. G. Gomez, and D. Gorman-Lewis. 2022. "Mineralogy, morphology, and reaction kinetics of ureolytic biocementation in the presence of seawater ions and varying soil materials." *Sci. Rep.* 12 (1): 17100. https://doi.org/10.1038/s41598-022-21268-3.

Carey, T. J., N. Stone, and B. L. Kutter. 2020. "Grain size analysis and maximum and minimum dry density testing of Ottawa F-65 sand for LEAP-UCD-2017." In *Model tests and numerical simulations of liquefaction and lateral spreading*, 31–44. Cham, Switzerland: Springer.

Cheng, L., R. Cord-Ruwisch, and M. A. Shahin. 2013. "Cementation of sand soil by microbially induced calcite precipitation at various degrees of saturation." *Can. Geotech. J.* 50 (1): 81–90. https://doi.org/10.1139/cgj-2012-0023.

Colombani, J. 2016. "The alkaline dissolution rate of calcite." *J. Phys. Chem. Lett.* 7 (13): 2376–2380.

Cubillas, P., S. Köhler, M. Prieto, C. Chaïrat, and E. H. Oelkers. 2005. "Experimental determination of the dissolution rates of calcite, aragonite, and bivalves." *Chem. Geol.* 216 (1–2): 59–77. https://doi.org/10.1016/j.chemgeo.2004.11.009.

DeJong, J. T., M. B. Fritzges, and K. Nüsslein. 2006. "Microbially induced cementation to control sand response to undrained shear." *J. Geotech. Geoenviron. Eng.* 132 (11): 1381–1392. https://doi.org/10.1061/(ASCE)1090-0241(2006)132:11(1381).

DeJong, J. T., M. G. Gomez, A. C. San Pablo, C. M. R. Graddy, D. C. Nelson, M. Lee, K. Ziotopoulou, M. El Kortbawi, B. Montoya, and T. H. Kwon. 2022. "State of the art: MICP soil improvement and its application to liquefaction hazard mitigation." In *Proc., 20th Int. Conf. on Soil Mechanics and Geotechnical Engineering*, 105. London: International Society for Soil Mechanics and Geotechnical Engineering.

DeJong, J. T., B. M. Mortensen, B. C. Martinez, and D. C. Nelson. 2010. "Bio-mediated soil improvement." *Ecol. Eng.* 36 (2): 197–210. https://doi.org/10.1016/j.ecoleng.2008.12.029.

DeJong, J. T., K. Soga, E. Kavazanjian, S. Burns, L. van Paassen, A. Al Qabany, and C. Y. Chen. 2013. "Biogeochemical processes and geotechnical applications: Progress, opportunities and challenges." In *Proc., 17th Géotechnique Symp. in Print*, 143–157. London: ICE Publishing.

Ebigbo, A., A. Phillips, R. Gerlach, R. Helmig, A. B. Cunningham, H. Class, and L. H. Spangler. 2012. "Darcy-scale modeling of microbially induced carbonate mineral precipitation in sand columns." *Water Resour. Res.* 48 (7): 1–17. https://doi.org/10.1029/2011WR011714.

Ferris, F. G., L. G. Stehmeier, A. Kantzas, and F. M. Mourits. 1997. "Bacteriogenic mineral plugging." *J. Can. Pet. Technol.* 36 (9): 56–61. https://doi.org/10.2118/97-09-07.

Fujita, Y., G. D. Redden, J. S. Ingram, M. M. Cortez, and R. W. Smith. 2004. "Strontium incorporation into calcite generated by bacterial ureolysis." *Geochim. Cosmochim. Acta* 68 (15): 3261–3270. https://doi.org/10.1016/j.gca.2003.12.018.

Gal, J. Y., Y. Fovet, and N. Gache. 2002. "Mechanisms of scale formation and carbon dioxide partial pressure influence. Part I. Elaboration of an experimental method and a scaling model." *Water Res.* 36 (3): 755–763. https://doi.org/10.1016/S0043-1354(01)00270-6.

Gehlen, M., F. C. Bassinot, L. Chou, and D. McCorkle. 2005. "Reassessing the dissolution of marine carbonates: II. Reaction kinetics." *Deep-Sea Res. I: Oceanogr. Res. Pap* 52 (8): 1461–1476.

Gomez, M. G., C. M. Anderson, C. M. R. Graddy, J. T. DeJong, D. C. Nelson, and T. R. Ginn. 2017. "Large-scale comparison of bioaugmentation and biostimulation approaches for biocementation of sands." *J. Geotech. Geoenviron. Eng.* 143 (5): 04016124. https://doi.org/10.1061/(ASCE)GT.1943-5606.0001640.

Gomez, M. G., and J. T. DeJong. 2017. "Engineering properties of biocementation improved sandy soils." In *Proc., of Grouting 2017*, 22–33. Reston, VA: ASCE.

Gomez, M. G., C. M. Graddy, J. T. DeJong, and D. C. Nelson. 2019. "Biogeochemical changes during bio-cementation mediated by stimulated and augmented ureolytic microorganisms." *Sci. Rep.* 9 (1): 1–15. https://doi.org/10.1038/s41598-019-47973-0.

Gomez, M. G., C. M. Graddy, J. T. DeJong, D. C. Nelson, and M. Tsesarsky. 2018. "Stimulation of native microorganisms for biocementation in samples recovered from field-scale treatment depths." *J. Geotech. Geoenviron. Eng.* 144 (1): 04017098. https://doi.org/10.1061/(ASCE)GT.1943-5606.0001804.

Gomez, M. G., B. C. Martinez, J. T. DeJong, C. E. Hunt, L. A. deVlaming, D. W. Major, and S. M. Dworatzek. 2015. "Field-scale bio-cementation tests to improve sands." *Proc. Inst. Civ. Eng. Ground Improv.* 168 (3): 206–216. https://doi.org/10.1680/grim.13.00052.

Gowthaman, S., A. Mohsenzadeh, K. Nakashima, H. Nakamura, and S. Kawasaki. 2020a. "Evaluation on the performance of MICP treated slope soil under acid rain environment." In *Proc., 10th Int. Conf. on Geotechnique, Construction Materials and Environment (GEOMATE 2020)*, 11–13. Melbourne, VIC, Australia: GEOMATE International Society.

Gowthaman, S., K. Nakashima, and S. Kawasaki. 2020b. "Freeze-thaw durability and shear responses of cemented slope soil treated by microbial induced carbonate precipitation." *Soils Found.* 60 (4): 840–855. https://doi.org/10.1016/j.sandf.2020.05.012.

Karol, R. H. 2003. *Chemical grouting and soil stabilization, revised and expanded*. Boca Raton, FL: CRC Press.

Khodadadi, T. H., E. Kavazanjian, and H. Bilsel. 2017. "Mineralogy of calcium carbonate in MICP-treated soil using soaking and injection treatment methods." In *Geotechnical Frontiers 2017: Transportation Facilities, Structures, and Site Investigation*, Geotechnical Special Publication 227, edited by T. L. Brandon and R. J. Valentine, 195–201. Reston, VA: ASCE.

Knorst, M. T., R. Neubert, and W. Wohlrab. 1997. "Analytical methods for measuring urea in pharmaceutical formulations." *J. Pharm. Biomed. Anal.* 15 (11): 1627–1632. https://doi.org/10.1016/S0731-7085(96)01978-4.

Lee, M., M. G. Gomez, M. El Kortbawi, and K. Ziotopoulou. 2022. "Evaluating the liquefaction triggering and post-triggering behavior of lightly cemented sands using microbially induced calcite precipitation (MICP)." *J. Geotech. Geoenviron. Eng.* 148 (1): 04021170. https://doi.org/10.1061/(ASCE)GT.1943-5606.0002707.

Lee, M., C. M. Kolbus, A. D. Yepez, and M. G. Gomez. 2019. "Investigating ammonium by-product removal following stimulated ureolytic microbially-induced calcite precipitation." In *Geo-Congress 2019: Soil Improvement*, Geotechnical Special Publication 309, edited by C. L. Meehan, S. Kumar, M. A. Pando, and J. T. Coe, 260–272. Reston, VA: ASCE.

Lin, H., M. T. Suleiman, H. M. Jabbour, and D. G. Brown. 2020. "Investigation of pore-scale $CaCO_3$ distributions and their effects on stiffness and permeability of sands treated by microbially induced carbonate precipitation (MICP)." *Soils Found.* 60 (4): 944–961. https://doi.org/10.1016/j.sandf.2020.07.003.

Lin, H., M. T. Suleiman, H. M. Jabbour, D. G. Brown, and E. Kavazanjian Jr. 2016. "Enhancing the axial compression response of pervious concrete ground improvement piles using biogrouting." *J. Geotech. Geoenviron. Eng.* 142 (10): 04016045. https://doi.org/10.1061/(ASCE)GT.1943-5606.0001515.

Martinez, B., J. DeJong, T. Ginn, B. Montoya, T. Barkouki, C. Hunt, B. Tanyu, and D. Major. 2013. "Experimental optimization of microbial-induced carbonate precipitation for soil improvement." *J. Geotech. Geoenviron. Eng.* 139 (4): 587–598. https://doi.org/10.1061/(ASCE)GT.1943-5606.0000787.

Martinez, B. C., and J. T. DeJong. 2009. "Bio-mediated soil improvement: Load transfer mechanisms at the micro-and macro-scales." In *Advances in Ground Improvement: Research to Practice in the United States and China*, Geotechnical Special Publication 188, edited by J. Han, G. Zheng, V. R. Schaefer, and M. Huang, 242–251. Reston, VA: ASCE.

Martinez, B. C., J. T. DeJong, and T. R. Ginn. 2014. "Bio-geochemical reactive transport modeling of microbial induced calcite precipitation to predict the treatment of sand in one-dimensional flow." *Comput. Geotech.* 58 (May): 1–13. https://doi.org/10.1016/j.compgeo.2014.01.013.

Minto, J. M., R. J. Lunn, and G. El Mountassir. 2019. "Development of a reactive transport model for field-scale simulation of microbially induced carbonate precipitation." *Water Resour. Res.* 55 (8): 7229–7245. https://doi.org/10.1029/2019WR025153.

Mitchell, J. K., and R. Kelly. 2013. "Addressing some current challenges in ground improvement." *Proc. Inst. Civ. Eng. Ground Improv.* 166 (3): 127–137. https://doi.org/10.1680/grim.12.00030.

Montoya, B. M., and J. T. DeJong. 2015. "Stress-strain behavior of sands cemented by microbially induced calcite precipitation." *J. Geotech. Geoenviron. Eng.* 141 (6): 04015019. https://doi.org/10.1061/(ASCE)GT.1943-5606.0001302.

Montoya, B. M., J. T. DeJong, and R. W. Boulanger. 2013. "Dynamic response of liquefiable sand improved by microbial-induced calcite precipitation." *Géotechnique* 63 (4): 302–312. https://doi.org/10.1680/geot.SIP13.P.019.

Morse, J. W., and R. S. Arvidson. 2002. "The dissolution kinetics of major sedimentary carbonate minerals." *Earth Sci. Rev.* 58 (1–2): 51–84. https://doi.org/10.1016/S0012-8252(01)00083-6.

Morse, J. W., and R. A. Berner. 1972. "Dissolution kinetics of calcium carbonate in sea water; I, A kinetic origin for the lysocline." *Am. J. Sci.* 272 (9): 840–851. https://doi.org/10.2475/ajs.272.9.840.

Mu, B., Z. Gui, F. Lu, E. Petropoulos, and Y. Yu. 2021. "Microbial induced carbonate precipitation improves physical and structural properties of Nanjing ancient city walls." *Materials* 14 (19): 5665. https://doi.org/10.3390/ma14195665.

Nassar, M. K., D. Gurung, M. Bastani, T. R. Ginn, B. Shafei, M. G. Gomez, C. M. R. Graddy, D. C. Nelson, and J. T. DeJong. 2018. "Large-scale experiments in microbially induced calcite precipitation (MICP): Reactive transport model development and prediction." *Water Resour. Res.* 54 (1): 480–500. https://doi.org/10.1002/2017WR021488.

O'Donnell, S. T., E. Kavazanjian Jr., and B. E. Rittmann. 2017. "MIDP: Liquefaction mitigation via microbial denitrification as a two-stage process. II: MICP." *J. Geotech. Geoenviron. Eng.* 143 (12): 04017095. https://doi.org/10.1061/(ASCE)GT.1943-5606.0001806.

Parkhurst, D. L., and C. A. J. Appelo. 2013. *Description of input and examples for PHREEQC version 3: A computer program for speciation,*

batch-reaction, one-dimensional transport, and inverse geochemical calculations. Rep. No. 6-A43. Reston, VA: USGS.

Phillips, A. J., et al. 2016. "Fracture sealing with microbially-induced calcium carbonate precipitation: A field study." *Environ. Sci. Technol.* 50 (7): 4111–4117. https://doi.org/10.1021/acs.est.5b05559.

Pinske, M. A. 2011. "Life cycle assessment of ground improvement methods." M.S. thesis, Dept. of Civil and Environmental Engineering, Univ. of California.

Plummer, L. N., and E. Busenberg. 1982. "The solubilities of calcite, aragonite and vaterite in CO_2-H_2O solutions between 0 and 90 C, and an evaluation of the aqueous model for the system $CaCO_3$-CO_2-H_2O." *Geochim. Cosmochim. Acta* 46 (6): 1011–1040. https://doi.org/10.1016/0016-7037(82)90056-4.

Raymond, A. J., M. A. Pinkse, A. Kendall, and J. T. DeJong. 2017. "Life-cycle assessment of ground improvement alternatives for the Treasure Island, California, redevelopment." In *Geotechnical Frontiers 2017: Waste Containment, Barriers, Remediation, and Sustainable Geoengineering*, Geotechnical Special Publication 276, edited by T. L. Brandon and R. J. Valentine, 345–354. Reston, VA: ASCE.

Ribeiro, B. G. O., and M. G. Gomez. 2022. "Investigating the dissolution behavior of calcium carbonate bio-cemented sands." In *Geo-Congress 2022: Soil Improvement*, Geotechnical Special Publication 331, edited by A. Lemnitzer and A. W. Stuedlein, 385–395. Reston, VA: ASCE.

San Pablo, A. C., et al. 2020. "Meter-scale biocementation experiments to advance process control and reduce impacts: Examining spatial control, ammonium by-product removal, and chemical reductions." *J. Geotech. Geoenviron. Eng.* 146 (11): 04020125. https://doi.org/10.1061/(ASCE)GT.1943-5606.0002377.

Seagren, E. A., and A. H. Aydilek. 2010. "Biomediated geomechanical processes." In *Environmental microbiology*. 2nd ed., 319–348. Hoboken, NJ: John Wiley & Sons.

Sjöberg, E. L., and D. Rickard. 1984. "Temperature dependence of calcite dissolution kinetics between 1 and 62°C at pH 2.7 to 8.4 in aqueous solutions." *Geochim. Cosmochim. Acta* 48 (3): 489–493. https://doi.org/10.1016/0016-7037(84)90276-X.

Smith, R. W., Y. Fujita, S. S. Hubbard, and T. R. Ginn. 2012. *Field investigations of microbially facilitated calcite precipitation for immobilization of strontium-90 and other trace metals in the subsurface*, 1–20. Washington, DC: US DOE.

Sposito, G. 2008. *The chemistry of soils*. Oxford, UK: Oxford University Press.

Stocks-Fischer, S., J. K. Galinat, and S. S. Bang. 1999. "Microbiological precipitation of $CaCO_3$." *Soil Biol. Biochem.* 31 (11): 1563–1571. https://doi.org/10.1016/S0038-0717(99)00082-6.

Stumm, W., and J. J. Morgan. 2012. Vol. 126 of *Aquatic chemistry: Chemical equilibria and rates in natural waters*. New York: Wiley.

Sun, X., L. Miao, H. Wang, R. Chen, and X. Guo. 2021. "Improvement of characteristics and freeze-thaw durability of solidified loess based on microbially induced carbonate precipitation." *Bull. Eng. Geol. Environ.* 80 (6): 4957–4966. https://doi.org/10.1007/s10064-021-02241-2.

Tobler, D. J., E. Maclachlan, and V. R. Phoenix. 2012. "Microbially mediated plugging of porous media and the impact of differing injection strategies." *Ecol. Eng.* 42 (May): 270–278. https://doi.org/10.1016/j.ecoleng.2012.02.027.

van Paassen, L. A. 2011. "Bio-mediated ground improvement: From laboratory experiment to pilot applications." In *Geo-Frontiers 2011 Technical Papers*, Geotechnical Special Publication 211, edited by J. Han, and D. E. Alzamora, 4099–4108. Reston, VA: ASCE.

Zamani, A., and B. M. Montoya. 2018. "Undrained monotonic shear response of MICP-treated silty sands." *J. Geotech. Geoenviron. Eng.* 144 (6): 04018029. https://doi.org/10.1061/(ASCE)GT.1943-5606.0001861.